INSTITUTE OF NATURAL AND APPLIED SCIENCES
UNIVERSITY OF CUKUROVA

MSc THESIS

Ahmet AYDIN

APPLICATIONS OF MEDICAL IMAGE PROCESSING TECHNIQUES ON A BIOMECHANICS SYSTEM

DEPARTMENT OF ELECTRICAL AND ELECTRONICS ENGINEERING

ADANA, 2009

ÇUKUROVA ÜNİVERSİTESİ
FEN BİLİMLERİ ENSTİTÜSÜ

MEDİKAL GÖRÜNTÜ İŞLEME TEKNİKLERİNİN BİYOMEKANİK BİR SİSTEME UYGULANMASI

Ahmet AYDIN

YÜKSEK LİSANS TEZİ
ELEKTRİK - ELEKTRONİK MÜHENDİSLİĞİ ANABİLİM DALI

Bu tez 28.08.2009 tarihinde aşağıdaki jüri üyeleri tarafından oybirliği ile kabul edilmiştir.

İmza.....
Yrd. Doç. Dr. Turgay İBRİKÇİ
DANIŞMAN

İmza.....
Prof. Dr. İbrahim D. AKÇALI
ÜYE

İmza.....
Yrd. Doç. Dr. M.Kerem ÜN
ÜYE

Bu tez Enstitümüz Elektrik - Elektronik Mühendisliği Anabilim Dalında hazırlanmıştır.
Kod No:

Prof. Dr. Aziz ERTUNÇ
Enstitü Müdürü
İmza ve Mühür

Bu Çalışma Ç.Ü. Bilimsel Araştırma Projeleri Birimi ve Kısmen de Tübitak 106M466 Numaralı Proje Tarafından Desteklenmiştir.

Proje No: MMF 2009 YL20

Not: Bu tezde kullanılan özgün ve başka kaynaktan yapılan bildirişlerin, çizelge, şekil ve fotoğrafların kaynak gösterilmeden kullanımı, 5846 sayılı Fikir ve Sanat Eserleri Kanunundaki hükümlere tabidir.

ABSTRACT

MSc THESIS

APPLICATIONS OF MEDICAL IMAGE PROCESSING TECHNIQUES ON A BIOMECHANICS SYSTEM

Ahmet AYDIN

DEPARTMENT OF ELECTRICAL AND ELECTRONICS ENGINEERING
INSTITUTE OF NATURAL AND APPLIED SCIENCES
UNIVERSITY OF ÇUKUROVA

Supervisor: Assist. Prof. Dr. Turgay İBRİKÇİ
Year: 2009, Pages: 48
Jury: Assist. Prof. Dr. Turgay İBRİKÇİ
Prof. Dr. İbrahim D. AKÇALI
Assist. Prof. Dr. M.Kerem ÜN

In the field of orthopedics treatment of extremity deformities can be realized by means of external fixators. But control of this biomedical system is very difficult. A mathematical model has been developed to improve quality of this service. Most of the parameters which are used in this theory have been obtained from two orthogonal medical images; one from Antero-Posterior, *AP*, direction and the other from lateral, *L*, direction. The quality of the results of this theory is dependent on the accuracy of the input parameters. Measuring these parameters takes a lot of time and accuracy of the results are low. The aim of this study is to prepare a software to make these measurements automatically and faster, to increase the accuracy of the results and thereby contrubuting to the improved accuracy of the calculations associated with the mathematical model.

Key Words: Fixator, medical image, image processing, inverse kinematics

ÖZ

YÜKSEK LİSANS TEZİ

MEDİKAL GÖRÜNTÜ İŞLEME TEKNİKLERİNİN BİYOMEKANİK BİR SİSTEME UYGULANMASI

Ahmet AYDIN

ÇUKUROVA ÜNİVERSİTESİ
FEN BİLİMLERİ ENSTİTÜSÜ
ELEKTRİK - ELEKTRONİK MÜHENDİSLİĞİ ANABİLİM DALI

Danışman: Yrd. Doç. Dr. Turgay İBRİKÇİ
Yıl: 2009, Sayfa: 48
Jüri: Yrd. Doç. Dr. Turgay İBRİKÇİ
Prof. Dr. İbrahim D. AKÇALI
Yrd. Doç. Dr. M.Kerem ÜN

Ortopedi alanında ekstremite kırıkların tedavisinde eksternal fiksatörler kullanılmaktadır. Fakat eksternal fiksatör olarak adlandırılan bu biyomekanik yapının kontrolü çok zordur. Bu işin daha doğru şekilde yapılabilmesi için bir matematik model geliştirilmistir. Bu modelde parametre olarak kullanılan verilerin bir çoğu sistemin birbirine dik, biri karşıdan (*AP*) ve diğeri dış yandan *L*, çekilmiş iki röntgen filminden elde edilmektedir. Bu modelin vereceği sonuçların kalitesi verilerin hassas bir şekilde elde edilmesine bağlıdır. Fakat bu verilerin manuel bir ekilde okunması hem çok uzun zaman almakta hemde verilerin beklenilen hassasiyette alınamamasına yol açmaktadır. Yapılan bu çalışmanın amacı yukarıda tarif edilen verilerin okunması işleminin otomatikleştirilip hızlandırılması, sonuçların kalitesinin arttırılması ve matematik modeldeki hesaplamaların yapılabilmesi amacıyla bir yazılımın hazırlanmasıdır.

Anahtar Kelimeler: Fixatör, medikal resim, görüntü işleme, ters kinematik

ACKNOWLEDGEMENTS

I would like to thank my supervisor Assist. Prof. Dr. Turgay İBRİKÇİ for his support. His help and suggestions are very important for me.

I would like to thank Prof. Dr. İbrahim Deniz AKÇALI for his scientific support, ideas and suggestions.

Further on I would like to thank Assist. Prof. Dr. Kerem ÜN for his comments and suggestions.

I would like to thank M. Onur ŞAHLAR for his help on preparing medical images.

Finally I would like to thank my family for their encouragement and all support.

TABLE OF CONTENTS **PAGE**

ABSTRACT I

ÖZ II

ACKNOWLEDGEMENTS III

TABLE OF CONTENTS IV

LIST OF TABLES VI

LIST OF FIGURES VII

1 INTRODUCTION 1

1.1 Definition of External Fixator 1

1.2 Aim of the Fixator Automation 1

2 INVERSE KINEMATICS OF BIOMECHANICAL SYSTEM 4

2.1 View - Position Relations 4

2.2 View-Position Relations of Biomechanical System 7

3 MATERIAL AND METHODS 18

3.1 Image Processing 18

3.1.1 Convolution 18

3.1.2 Sobel Edge Detector 19

3.1.3 Binary Large Object Analysis 20

3.1.4 Thresholding and Inverting 22

3.2 Inverse Kinematic Studies 22

3.2.1 Preparing X-Ray Images 22

3.2.2 Measuring Theorical Inputs From Medical Image 23

3.2.3 Obtaining Clinical Data 25

3.2.4 Evaluating The Results 25

3.3 Fixator Automation Software 26

4 RESULTS and DISCUSSIONS 31
4.1 Verifying the Mathematical Theory 31
4.1.1 Case 1 31
4.1.2 Case 2 32
4.1.3 Case 3 33
4.2 Measurement Experiments With Fixator Automation Software 35
4.2.1 Measurement 1 35
4.2.2 Measurement 2 40

5 CONCLUSION 45

REFERENCES 46

CURRICULUM VITAE 48

LIST OF TABLES **PAGE**

Table 4.1 Original link lengths for measurement 1 35
Table 4.2 Link lengths for initial state of measurement 1 37
Table 4.3 Link lengths for aligned state of measurement 1 37
Table 4.4 Original link lengths for measurement 2 40
Table 4.5 Link lengths for initial state of measurement 2 44
Table 4.6 Link lengths for aligned state of measurement 2 44

LIST OF FIGURES **PAGE**

Figure 1.1 External fixator 2

Figure 2.1 View - position relations 5
Figure 2.2 View-position relations of biomechanical system 9
Figure 2.3 View-position relations of biomechanical system for *L*-view 10
Figure 2.4 View-position relations of biomechanical system for *AP*-view 11
Figure 2.5 View-position relations of biomechanical system for *Ax*-view 12
Figure 2.6 SPM, proximal and distal ring views 13

Figure 3.1 A small image (a) and an kernel (b) to illustrate convolution 18
Figure 3.2 Sobel operator 19
Figure 3.3 A gray scale image and after it is filtered with Sobel operator 20
Figure 3.4 A binary image and the result of blob analysis on detecting different objects 21
Figure 3.5 Vidar medical image digitizer 23
Figure 3.6 The *AP* image and software interface 27
Figure 3.7 The filtered *AP* image 28
Figure 3.8 The measured *AP* image 30
Figure 3.9 The measured *L* image and calculation results 30

Figure 4.1 Case 1 of fixator assembly 32
Figure 4.2 Case 2 of fixator assembly 33
Figure 4.3 Case 3 of fixator assembly 34
Figure 4.4 The *AP* (a), *L* (b) and Axial (c) images for measurement 1 36
Figure 4.5 The automatic measurement results of *AP* for measurement 1 38
Figure 4.6 The automatic measurement results of *L* for measurement 1 39
Figure 4.7 The *AP* (a), *L* (b) and Axial (c) images for measurement 2 41
Figure 4.8 The automatic measurement results of *AP* for measurement 2 42
Figure 4.9 The automatic measurement results of *L* for measurement 2 43

1. INTRODUCTION

1.1 Definition of External Fixator

In the book titled "Concepts in External Fixation" (Seligson and Pope, 1982), external fixator is defined as a mechanical system which can be used to remove instabilty of bone fragments externally by connecting one or more bars to the bone to compose a comprehensive frame. Hippocrates, 2500 years ago, used the external fixator for the first time to treat tibia fractures and then this system generalized with studies of Malgaigne in 1840, Parkhill in 1894 and Della Mano in 1938, (Eren and Eralp, 1999)–(Parkhill, 1897). Later in time, external fixators started to lose its popularity because of the bad results originated from wrong use of the mechanical system. However with the studies of Burny (Burny et al., 1982) and other researchers on the fixator mechanics improve the success of the system and it generalized again, (Behrens, 1981)– (Fernandez, 1985). The discovery of Ring Fixator to control the bone fragments in all directions by Ilizarov (Ilizarov and Green, 1992) is accepted as a big step for the practice of external fixation, (Çakmak and Kocaoğlu, 1999).

1.2 Aim of the Fixator Automation

In medical practice, management of extremity fractures and deformity corrections can be realized by means of external fixators, Figure 1.1. However, the quality of this service can only be improved through a biomechanical approach, in which a mathematical model is to be developed for the effective use of such orthopedic devices (Mutlu et al., 2006). Based on this idea, a project named as Fixator Automation has been started and supported by TUBITAK. Fundamentally, it will be shown, here in this project, how an external fixator can be deployed in order to bring the fractured bone fragments to their anatomically correct positions or to move the fragment ends in a controlled fashion. One of the spatial external fixators which can provide six degrees of freedom, three rotations and three translations, is based on the so-called Gough-Stewart or simply Stewart Platform Mechanisms. The most general and versatile type of Stewart Platform Mechanism, the so-called (6-6) type, is a robotic frame which consists of two platforms connected to each

other through six spherical joints (or three spherical and three universal joints) by six bars the lengths of which can be adjusted. The effective use of the mechanism as an external fixator will require the development of a mathematical theory in which radiogrophical data as well as clinical examination results are to be introduced as input and bar lengths are to be produced as output. On the other hand, the orthopedic surgeon will be directed by the results of the mathematical theory as to how to guide the fragment ends in accordance with a treatment strategy deemed suitable from a medical point of view. In order for this process to function smoothly, it is necessary that the input and output of the mathematical theory be perceived with sufficient accuracy and also be standardized as well. This, in turn, makes it obligatory that the radiogrophical films be scanned with precision and the clinical investigations be done by a digital camera with high resolution for an accurate and reliable acquisition of input to processed in a computer environment. The input data digitally collected and visually represented on the computer are further processed to be transformed into a standard form usable by the mathematical theory.

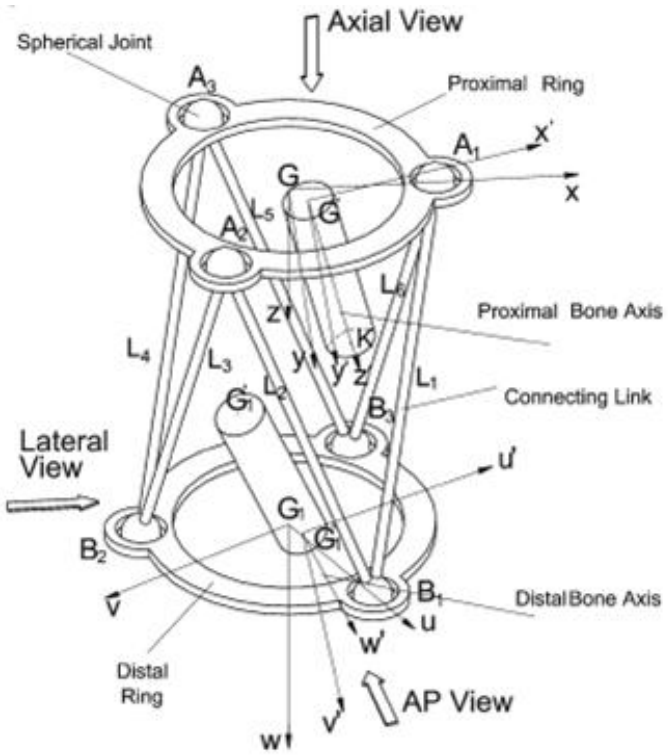


Figure 1.1 External fixator

To obtain these input data automatically, we should use image processing techniques applied to digitized X-Ray images to find the edges without noise and then use mathe-

matical algorithms, to measure these parameters from the input images. And the last goal of the project is to develop an expert system[1] which can be used to measure input data of the mathematical theory and calculate the link lengths for the initial condition and aligned condition of the fragments.

[1] Software that tries to regenerate the performance of one or more human experts, most commonly in a specific problem domain (Giarratano and Riley, 1994)

2. INVERSE KINEMATICS OF BIOMECHANICAL SYSTEM

Inverse kinematics is a kind of motion planning, it can be used to determine the parameters of a jointed flexible object for achieving a desired pose. Inverse kinematics of biomechanical system is a study of İbrahim Deniz Akçali which is prepared for 106M466 Tubitak Project (Akçali, 2007). All images in this section has been used with permission of İ. D. Akçali.

2.1 View - Position Relations

Towards formulation of the inverse kinematic problem one issue is to find the fundamental relationships between the position of a real object and its 2-D images. To this end, we chose a link in space with the axis designated by w and a cartesian xyz system located at its end, as shown in Figure 2.1. We look at the spatial bar once in the direction of x-axis to produce L-view, and in another time against the direction of y-axis to produce AP-image. If the length components of the link with the real length c along the x, y, z axes are represented by c_x, c_y, c_z and L, AP - image lengths by c_L, c_{AP} , respectively then the following relationships can be written from Figure 2.1:

$$c_x = c_z \tan \psi_{AP} \tag{2.1}$$

$$c_y = -c_z \tan \psi_L \tag{2.2}$$

$$c^2 = {c_x}^2 + {c_y}^2 + {c_z}^2 \tag{2.3}$$

$${c_{AP}}^2 = {c_x}^2 + {c_z}^2 \tag{2.4}$$

$${c_L}^2 = {c_y}^2 + {c_z}^2 \tag{2.5}$$

In equations 2.1 - 2.5, ψ_L and ψ_{AP} signify the angles between the z-axis and the link images in the L and AP views.

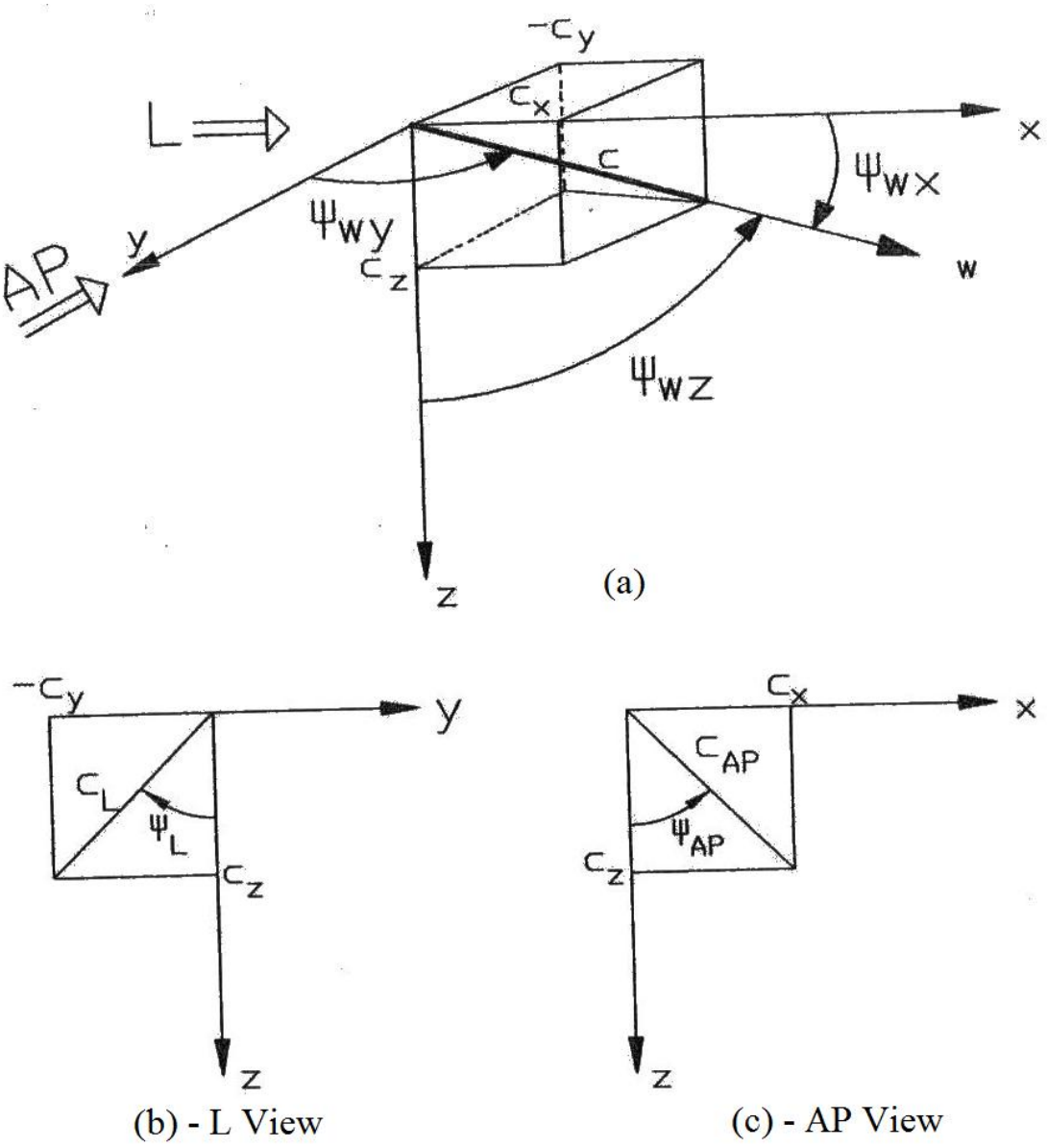


Figure 2.1 View - position relations

If the expressions 2.1 - 2.2 are substituted into 2.3 - 2.5, the following results are obtained:

$$c_z = \frac{c}{\sqrt{1+\tan^2\psi_{AP}+\tan^2\psi_L}} \tag{2.6}$$

$$c_z = c_{AP}\cos\psi_{AP} = c_L\cos\psi_L \tag{2.7}$$

$$c_x = c_L\cos\psi_L\tan\psi_{AP} \tag{2.8}$$

$$c_y = -c_L \cos\psi_L \tan\psi_L \tag{2.9}$$

$$c = c_{AP} \cos\psi_{AP} \sqrt{1 + \tan^2\psi_{AP} + \tan^2\psi_L} \tag{2.10}$$

Calling the angles between the w link axis and the x, y, z axes $\psi_{wx}, \psi_{wy}, \psi_{wz}$, which show the angular position of the link in space, then the following relationships can be written from Figure 2.1:

$$\cos\psi_{wx} = \frac{c_x}{c};\ \cos\psi_{wy} = \frac{c_y}{c};\ \cos\psi_{wz} = \frac{c_z}{c} \tag{2.11}$$

Evaluating the relationships 2.7 - 2.9 in equation 2.11 the following expressions result:

$$\cos\psi_{wx} = \frac{\tan\psi_{AP}}{\sqrt{1 + \tan^2\psi_{AP} + \tan^2\psi_L}} \tag{2.12}$$

$$\cos\psi_{wy} = \frac{-\tan\psi_L}{\sqrt{1 + \tan^2\psi_{AP} + \tan^2\psi_L}} \tag{2.13}$$

$$\cos\psi_{wz} = \frac{1}{\sqrt{1 + \tan^2\psi_{AP} + \tan\psi_L}} \tag{2.14}$$

The significance of the relationships above is to be able to calculate the real length c and the angular position of the link in 3-D space when data $c_L, c_{AP}, \psi_L, \psi_{AP}$ concerning the L and AP views can be measured. In this context, it will be possible to describe a unit vector e_w along the link axis by means of the unit vector components (e_{wx}, e_{wy}, e_{wz}) with reference to the x, y, z unit vectors (i, j, k).

Let a moving uvw system be coincident with the fixed xyz system at the beginning. The uvw system is rotated first about the x-axis by θ_x angle, then about the y-axis by θ_y angle, and finally about the z-axis by θ_z angle. The resulting composite transformation matrix is represented by the following rotation matrix:

$$\left[A_{xyz}^{uvw}\right] = rot\left[\theta_x, \theta_y, \theta_z\right] = \left[e_u, e_v, e_w\right] = \begin{bmatrix} e_{ux} & e_{vx} & e_{wx} \\ e_{uy} & e_{vy} & e_{wy} \\ e_{uz} & e_{vz} & e_{wz} \end{bmatrix} \tag{2.15}$$

In this equation $e_{ux}, e_{uy}, e_{uz}, e_{vx}, e_{vy}, e_{vz}, e_{wx}, e_{wy}, e_{wz}$ are the components of the unit vectors of u, v, w coordinate system (e_u, e_v, e_w) along the x, y, z axes; and $\left[A_{xyz}^{uvw}\right]$ is a transformation matrix which maps a vector defined in uvw coordinate system into the xyz coordinate system.

If the unit vector component (e_{wx}, e_{wy}, e_{wz}) defined by 2.12, 2.13, 2.14 relationships and the amount of rotation about z-axis (θ_z) are known, then it is easier to calculate angles θ_x and θ_y in the following way:

$$\overrightarrow{e_w} = \overrightarrow{i}\cos\psi_{wx} + \overrightarrow{j}\cos\psi_{wy} + \overrightarrow{k}\cos\psi_{wz} \tag{2.16}$$

$$\left[A_{xyz}^{uvw}\right] = \begin{bmatrix} \cos\theta_z\cos\theta_y & \cos\theta_z\sin\theta_y\sin\theta_x - \sin\theta_z\cos\theta_x & \cos\theta_z\sin\theta_y\cos\theta_x + \sin\theta_z\sin\theta_x \\ \sin\theta_z\cos\theta_y & \sin\theta_z\sin\theta_y\sin\theta_x + \cos\theta_z\cos\theta_x & \sin\theta_z\sin\theta_y\cos\theta_x - \cos\theta_z\sin\theta_x \\ -\sin\theta_y & \cos\theta_y\sin\theta_x & \cos\theta_y\cos\theta_x \end{bmatrix} \tag{2.17}$$

By comparing the relationships 2.15, 2.16 and 2.17 the following results are obtained:

$$\tan\theta_y = \frac{e_{wx}\cos\theta_z + e_{wy}\sin\theta_z}{e_{wz}} \tag{2.18}$$

$$\cos\theta_x = \frac{e_{wz}}{\cos\theta_y} \tag{2.19}$$

Upon calculation of θ_x, θ_y by means of equations 2.18 and 2.19 together with a knowledge of θ_z all the entries of the matrix 2.17 or 2.15 are to be fully determined. It is observed that, if we know the values of ψ_L, ψ_{AP} and the value of the angle of the rotation around z-axis (θ_z), we can calculate the transformation matrix defined in equations 2.15 or 2.17.

2.2 View-Position Relations of Biomechanical System

The biomechanical system under consideration consists of mechanical and biological components in which a (6-6) Stewart Platform Mechanism is used with the proximal and distal fragments attached rigidly to the base and moving platform, respectively, as

seen in Figure 2.2. The main purpose here is to find the real position of the 3-D biomechanical system from the images taken from different angles as many time as necessary. Departing from these findings, the next fundamental step is to determine the required setting of the mechanical system which will bring the proximal and distal fragments to their anatomically correct position. Two configurations of the mechanical system are of critical importance for the biological components. The first one corresponds to the instant configuration at the time when the images are recorded; the second one pertains to that position in which the proximal and distal fragments are aligned.

The world (xyz) coordinate system is selected at the center G of the proximal ring in such a way that the z-axis coincides with the normal of the ring, as seen in Figure 2.2. Another $x'y'z'$ coordinate system is chosen with its origin located at the center G' of the proximal fragment on the ring plane by which z' axis is directed along the fragment axis. The uvw coordinate system, in which w axis is perpendicular to the distal ring plane at the ring center G_1, is considered to be attached to the moving platform. The fourth coordinate system referred to as $u'v'w'$ is taken at the center $G_1{}''$ of the distal bone on the plane of the moving platform in such a way that the bone axis points along the w' axis. The mechanical parameters characterizing the Stewart Platform Mechanism are designated by $\alpha_1 - \alpha_6$, R, $\varepsilon_1 - \varepsilon_6$, R_1. Here R, R_1 are the radius of the proximal and distal rings, respectively. $\alpha_1 - \alpha_6$ define the angular locations of the spherical joints of the proximal ring while $\varepsilon_1 - \varepsilon_6$ define the angular positions of the universal joints on the distal ring, Figure 2.6. From now on, the subscript is used to signify the initial set of values at the time when bone fragments nonaligned; the subscript "n" will refer to the configuration in which the bone fragments are finally aligned. Based on the data set $(\psi_L, \psi_{AP}, \delta_0)$ and the theory of 2.1, the matrix $\left[A_{xyz}^{uvw}\right]_0$ showing the transformation between the moving uvw and the fixed xyz coordinate systems is determined. Here δ_0 represents the projected angle between the x and u axes, Figure 2.2, Figure 2.3, Figure 2.4, Figure 2.5.

In the second step, the same theory can be applied for w'-axis to find all entries of the $\left[A_{xyz}^{u'v'w'}\right]_0$ matrix, which represents the transformation between xyz and $u'v'w'$ systems, together with distal bone length c by using data set $(\beta_L, \beta_{AP}, \delta_{Ax}, c_L)$ whereby δ_{Ax} indicates the relative rotation angle between proximal and distal fragments, around z-axis, Figure 2.2, Figure 2.3, Figure 2.4, Figure 2.5.

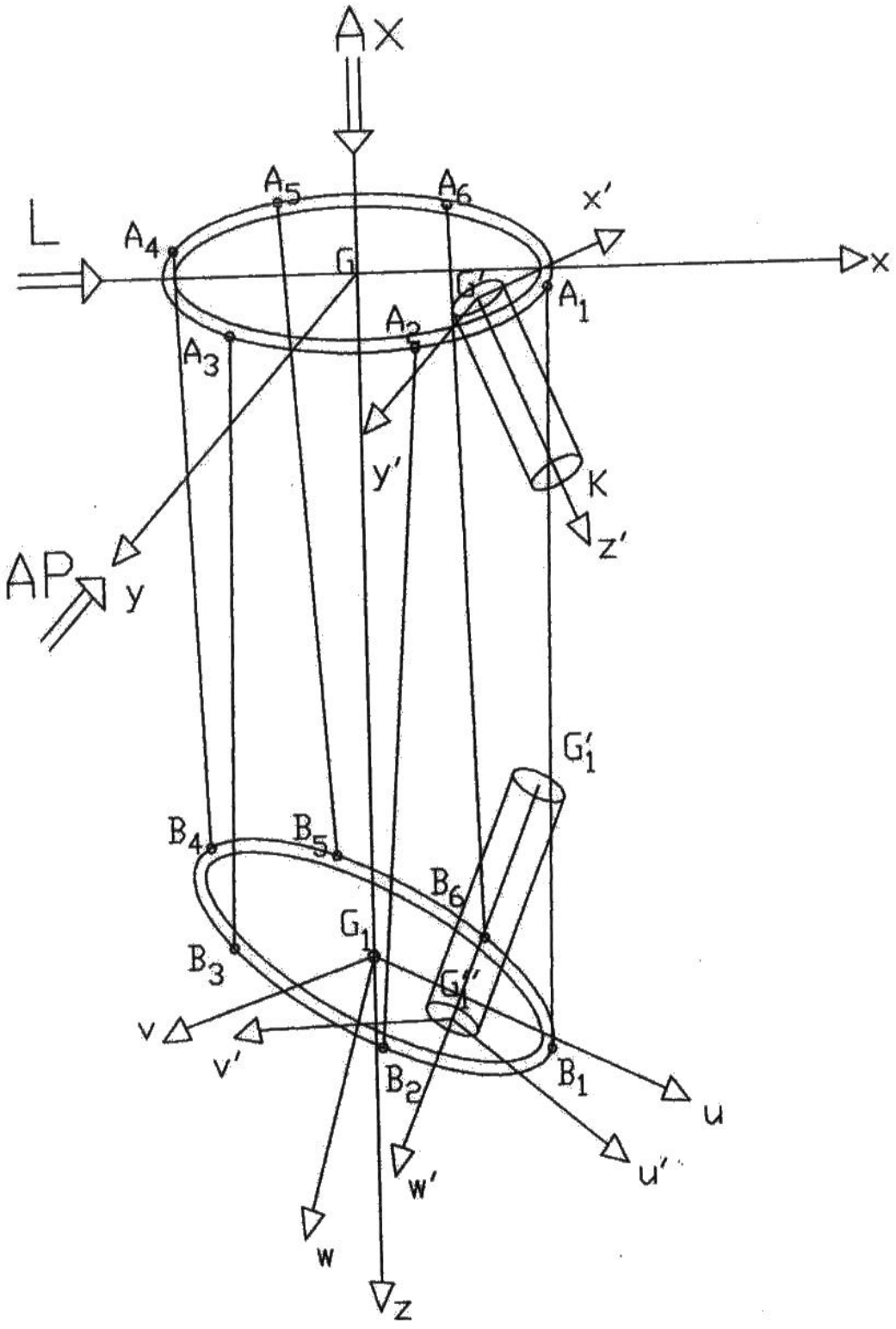


Figure 2.2 View-position relations of biomechanical system

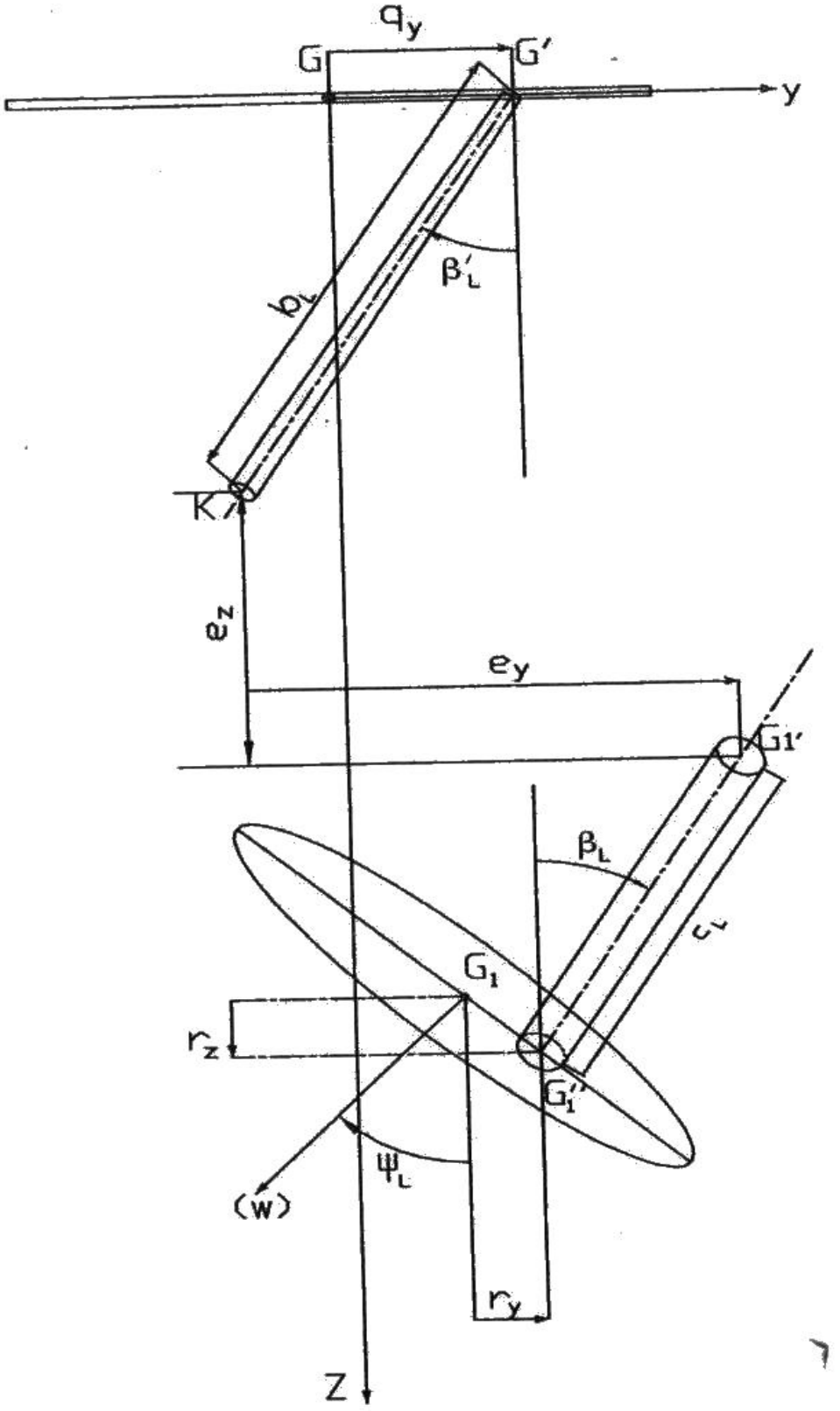


Figure 2.3 View-position relations of biomechanical system for *L*-view

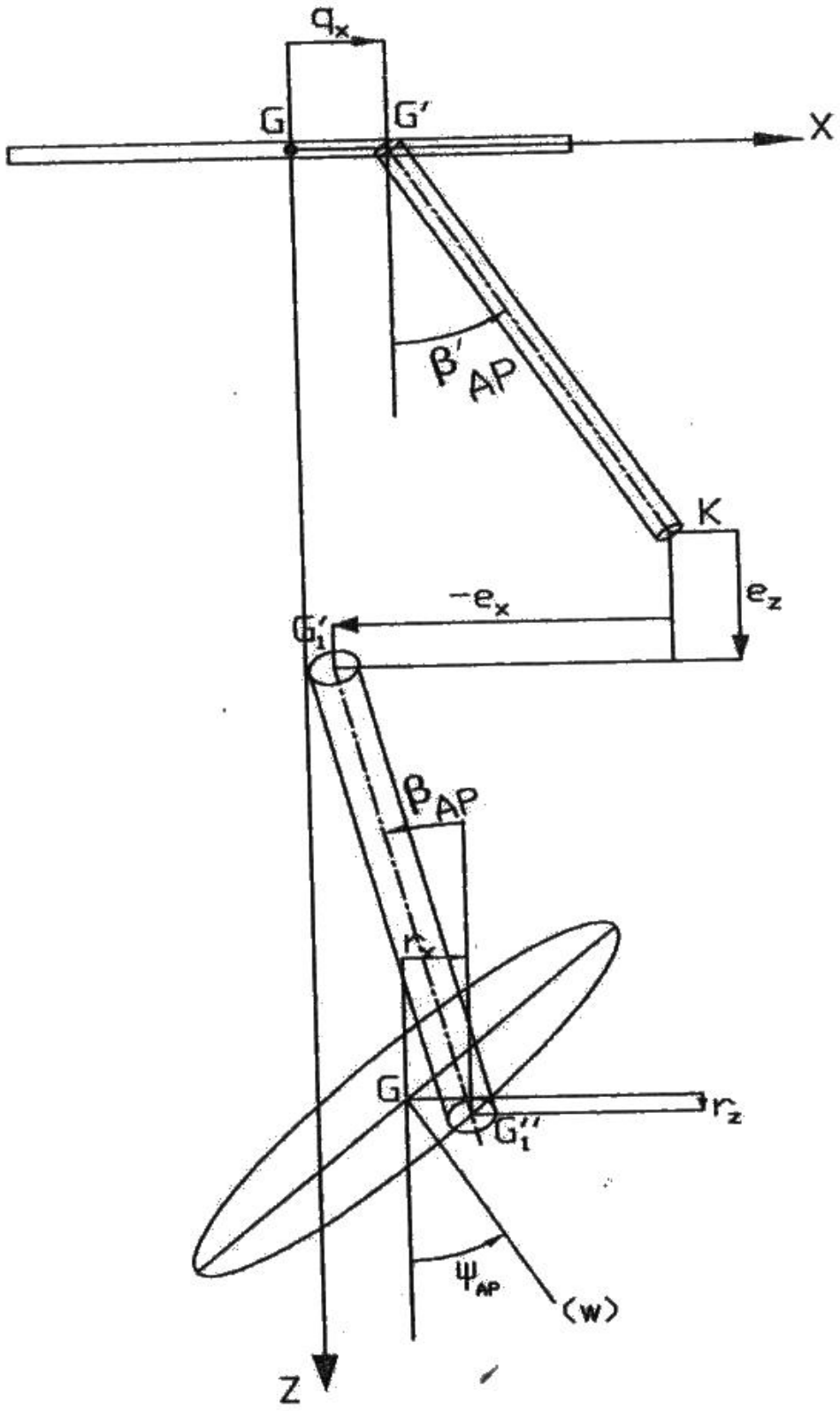


Figure 2.4 View-position relations of biomechanical system for *AP*-view

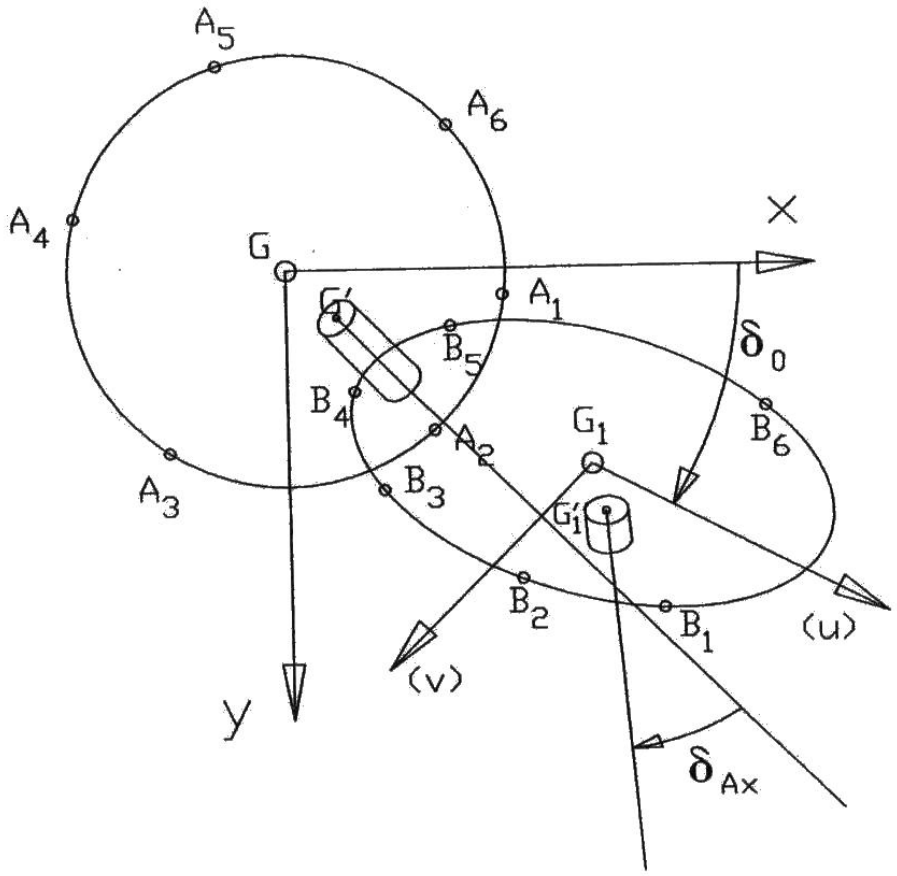


Figure 2.5 View-position relations of biomechanical system for *Ax*-view

At the third step, by assigning values $(\beta'_L, \beta'_{AP}, 0, b_L)$ to the input parameter set $(\theta_x, \theta_y, \theta_z, c)$ of the theory of 2.1, the transformation matrix $\left[A_{xyz}^{x'y'z'}\right]_0$, which represents the mapping from $x'y'z'$ system into the xyz system, together with proximal bone length b, Figure 2.3, Figure 2.4. At the fourth step, $\left[A_{uvw}^{u'v'w'}\right]_0$ matrix, which describes how the distal fragment is attached to the distal ring, can be calculated by utilizing orthonormal properties (Craig, 1989) - (Fu et al., 1987) of the rotation matrices:

$$\left[A_{uvw}^{u'v'w'}\right]_0 = \left[A_{xyz}^{uvw}\right]_0^{-1} \left[A_{xyz}^{u'v'w'}\right]_0 \tag{2.20}$$

or

$$\left[A_{uvw}^{u'v'w'}\right]_0 = \left[A_{xyz}^{uvw}\right]_0^{T} \left[A_{xyz}^{u'v'w'}\right]_0 \tag{2.21}$$

The superscript "T" denotes the transpose of the matrix.

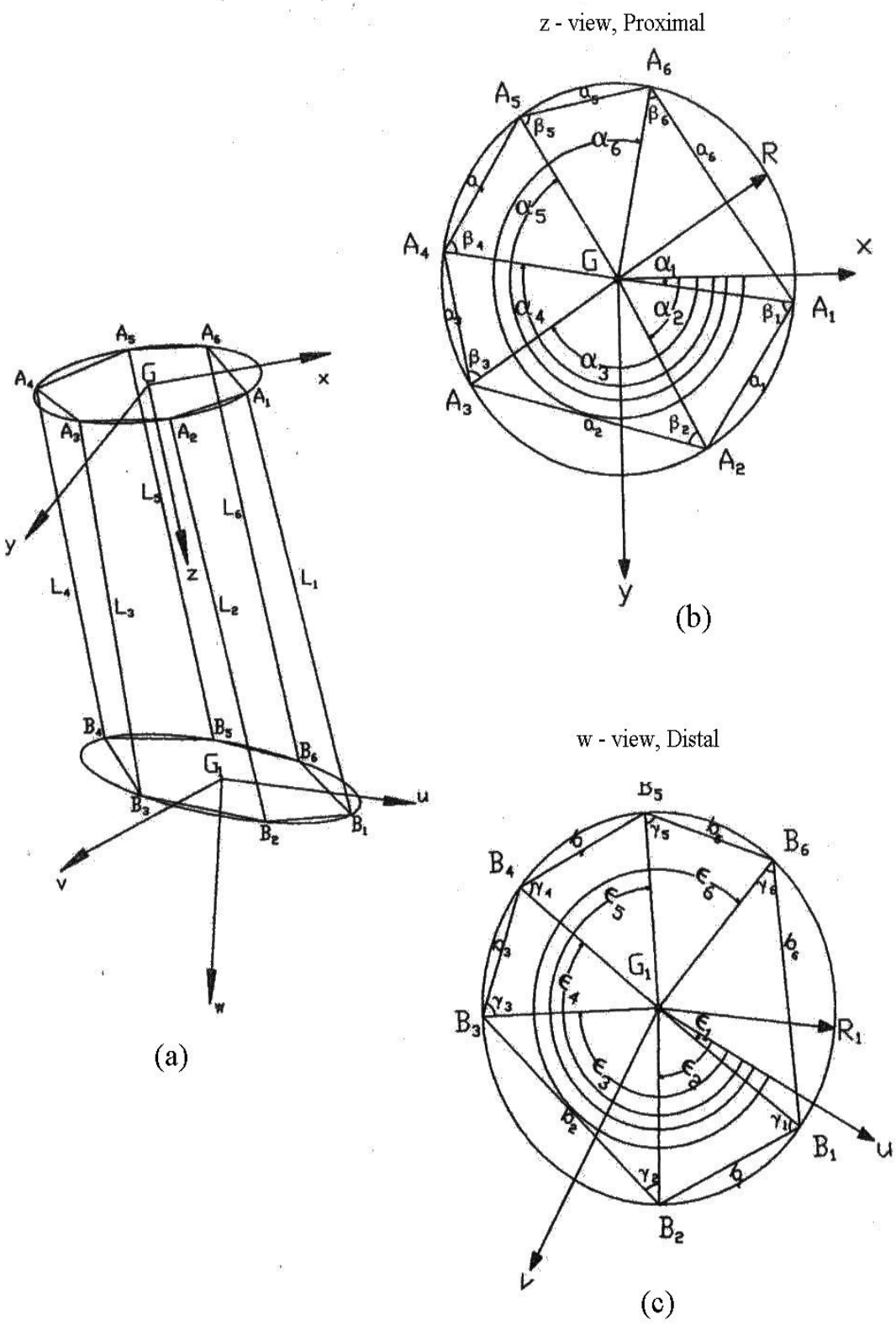


Figure 2.6 SPM, proximal and distal ring views

The next step of the theory is calculating the coordinates of joint points A_i $i = 1-6$ on the proximal ring plane, $(x_{A_i}, y_{A_i} \;\; i = 1-6)$, the local and world coordinates of the joint points on the distal ring plane B_i $i = 1-6$, (u_{B_i}, v_{B_i}), $x_{B_i}, y_{B_i}, z_{B_i}$, $\;i = 1-6$. In this way the lengths of the adjustable links for the initial configuration, L_i $i = 1-6$ will be determined. Thus, x_{A_i}, y_{A_i} are computed with a knowledge of the proximal ring radius (R), and angular positions of joints A_i $(\alpha_i \;\; i = 1-6)$ as shown below:

$$x_{A_i} = R\cos\alpha_i; \;\; y_{A_i} = R\sin\alpha_i \quad i = 1-6 \tag{2.22}$$

Similarly local joint coordinates on the moving plane are evaluated by knowing the radius of distal ring R_1 and angular positions of joints $(\varepsilon_i \;\; i = 1-6)$:

$$u_{B_i} = R_1\cos\varepsilon_i; \;\; v_{B_i} = R_1\sin\varepsilon_i \;\; i = 1-6 \tag{2.23}$$

From Figure 2.2 the following vector equation can be written:

$$\overrightarrow{GG_1} = \overrightarrow{GG'} + \overrightarrow{G'K} + \overrightarrow{KG'_1} + \overrightarrow{G'_1G''_1} - \overrightarrow{G_1G''_1} \tag{2.24}$$

and the vectors involved in the above equation can be expressed as:

$$\overrightarrow{GG'} = q_x\,\overrightarrow{i} + q_y\,\overrightarrow{j}; \;\; \overrightarrow{G'K} = b\,\overrightarrow{e_{z'}} \tag{2.25}$$

$$\overrightarrow{KG'_1} = e_x\,\overrightarrow{i} + e_y\,\overrightarrow{j} + e_z\,\overrightarrow{k}; \;\; \overrightarrow{G'_1G''_1} = c\,\overrightarrow{e_{w'}} \tag{2.26}$$

$$\overrightarrow{G_1G''_1} = r_x\,\overrightarrow{i} + r_y\,\overrightarrow{j} + r_z\,\overrightarrow{k} \tag{2.27}$$

In the preceding equations q_x, q_y denote the distances between the center of the proximal fragment and that of the proximal ring in the x, y directions; r_x, r_y, r_z are the distances between the center of distal fragment and that of the distal ring measured parallel to x, y, z axes; e_x, e_y, e_z are the relative translation of the fragment ends at the fracture site along the x, y, z directions; b and c are the lengths of the proximal and distal fragments; $\overrightarrow{e_{z'}}$ and $\overrightarrow{e_{w'}}$ are the unit vectors of z' and w' axes. All the vectors are now written in terms of the unit vectors of xyz system:

$$\overrightarrow{G'K} = b\left(e_{z'x}\overrightarrow{i} + e_{z'y}\overrightarrow{j} + e_{z'z}\overrightarrow{k}\right) \tag{2.28}$$

$$\overrightarrow{G'_1G''} = c\left(e_{w'x}\overrightarrow{i} + e_{w'y}\overrightarrow{j} + e_{w'z}\overrightarrow{k}\right) \tag{2.29}$$

$$\overrightarrow{G_1B_i} = \left(u_{B_i}e_{ux} + v_{B_i}e_{vx}\right)\overrightarrow{i} + \left(u_{B_i}e_{uy} + v_{B_i}e_{vy}\right)\overrightarrow{j} + \left(u_{B_i}e_{uz} + v_{B_i}e_{vz}\right)\overrightarrow{k} \quad i = 1-6 \tag{2.30}$$

$$\overrightarrow{GA_i} = x_{A_i}\overrightarrow{i} + y_{A_i}\overrightarrow{j} \quad i = 1-6 \tag{2.31}$$

$$\overrightarrow{GB_i} = \overrightarrow{GG_1} + \overrightarrow{G_1B_i} \quad i = 1-6 \tag{2.32}$$

$$L_i = |GA_i - GB_i|_0 \quad i = 1-6 \tag{2.33}$$

Up until this point the relationships between the parameters of the biological sub-assembly and the mechanical sub-assembly for nonaligned position have been determined. Some of the expressions written so far are related only to the nonaligned position except a few of them. So the unchanged parameters must be determined and the changed parameters must be calculated again, "n" will be used for changed parameters. After these explanations, before finding new parameter used for healthy position it is important to determine the unchanged parameters. The first of them is $\left[A_{uvw}^{u'v'w'}\right]_0$ matrix which found at 2.20 or 2.21 equations and used to define the conversation between uvw coordinate system and $u'v'w'$ coordinate system. It has known that the positions of top and bottom fragments don't change according to the top and bottom rings so these expressions can be written as:

$$\left[A_{uvw}^{u'v'w'}\right]_n = \left[A_{uvw}^{u'v'w'}\right]_0 \tag{2.34}$$

$$\left[A_{xyz}^{z'y'z'}\right]_n = \left[A_{xyz}^{x'y'z'}\right]_0 \tag{2.35}$$

And using the same idea when the system adjusted to the healthy position the coordinates of G''_1 (r_u, r_v) according to center of the distal ring (G_1) don't change in (uvw) coordinate system. So these relations can be written:

$$\left(\overrightarrow{G_1G''}\right)_0 = r_u\overrightarrow{e_{u0}} + r_v\overrightarrow{e_{v0}} = r_x\overrightarrow{i} + r_y\overrightarrow{j} + r_z\overrightarrow{k} \tag{2.36}$$

$$r_u = r_x e_{ux_0} + r_y e_{uy_0} + r_z e_{uz_0} \tag{2.37}$$

$$r_v = r_x e_{vx_0} + r_y e_{vy_0} + r_z e_{vz_0} \tag{2.38}$$

We know that proximal ring is stationary so we can say that coordinates of (G') (q_x, q_y) according to center of the proximal ring (G) don't change and besides of these the coordinates of joint points (x_{A_i}, y_{A_i}) and $(u_{B_i}, v_{B_i}\ \ i = 1-6)$ at top and bottom rings don't change in local coordinate system, too. In addition to unchanged parameters there are lots of parameters which will change for healthy position. One of the changed parameters is $\left[A_{xyz}^{uvw}\right]_n$ matrix which defines transformation between *uvw* and *xyz* coordinate system. Otherwise using properties of transformation matrices in healthy position this result is obtained:

$$\left[A_{xyz}^{u'v'w'}\right]_n = \left[A_{xyz}^{uvw}\right]_n \left[A_{uvw}^{u'v'w'}\right]_n \tag{2.39}$$

or

$$\left[A_{xyz}^{uvw}\right]_n = \left[A_{xyz}^{u'v'w'}\right]_n \left[A_{uvw}^{u'v'w'}\right]_n^T \tag{2.40}$$

The condition for top and bottom fragments being in the same anatomic axis is defined in this relation:

$$\left[A_{xyz}^{x'y'z'}\right]_n = \left[A_{xyz}^{u'v'w'}\right]_n \tag{2.41}$$

And now if 2.34, 2.35 and 2.41 are substituted in 2.40 this relationship can be obtained:

$$\left[A_{xyz}^{uvw}\right]_n = \left[A_{xyz}^{x'y'z'}\right]_0 \left[A_{uvw}^{u'v'w'}\right]_0 \tag{2.42}$$

This relation tells us how we must state the system for healthy position and it is an important relation because of it gives us the ability of finding healthy condition parameters from unhealthy condition parameters. At the final step, the length of the adjustment

screws for healthy position ($L_{in}\ \ i = 1-6$) must be calculated, so for this purpose this can be written:

$$\left(\overrightarrow{GG_1}\right)_n = \overrightarrow{GG'} + \overrightarrow{G'G''_1} - \left(\overrightarrow{G_1G''_1}\right)_n \tag{2.43}$$

here:

$$\overrightarrow{G'G''_1} = (b+c)\ \left(e_{z'x}\,\overrightarrow{i} + e_{z'y}\,\overrightarrow{j} + e_{z'z}\,\overrightarrow{k}\right) \tag{2.44}$$

$$\left(\overrightarrow{G_1G''_1}\right)_n = r_u\overrightarrow{e_{un}} + r_v\overrightarrow{e_{vn}} \tag{2.45}$$

or

$$\left(\overrightarrow{G_1G''_1}\right)_n = \left(r_u e_{ux_n} + r_v e_{vx_n}\right)\overrightarrow{i} + \left(r_u e_{uy_n} + r_v e_{vy_n}\right)\overrightarrow{j} + \left(r_u e_{uz_n} + r_v e_{vz_n}\right)\overrightarrow{k} \tag{2.46}$$

And these can be used:

$$\left(\overrightarrow{GB_i}\right)_n = \left(\overrightarrow{GG_1}\right)_n + \left(\overrightarrow{G_1B_i}\right)_n \quad i = 1-6 \tag{2.47}$$

$$\left(\overrightarrow{G_1B_i}\right)_n = u_{B_i}\overrightarrow{e_{u_n}} + v_{B_i}\overrightarrow{e_{v_n}} \tag{2.48}$$

or

$$\left(\overrightarrow{G_1B_i}\right)_n = \left(u_{B_i}e_{ux_n} + v_{B_i}e_{vx_n}\right)\overrightarrow{i} + \left(u_{B_i}e_{uy_n} + v_{B_i}e_{vy_n}\right)\overrightarrow{j} + \left(u_{B_i}e_{uz_n} + v_{B_i}e_{vz_n}\right)\overrightarrow{k} \tag{2.49}$$

and at the final $L_{i_n} = (A_iB_i)_n\ \ i = 1-6$ have been calculated:

$$L_{i_n} = |GA_i - GB_i|_n \tag{2.50}$$

3. MATERIAL AND METHODS

3.1 Image Processing

3.1.1 Convolution

Convolution is a mathematical operation which can be used for many prevalent image processing operators. Two arrays of numbers which have different sizes, but same dimensionality are multiplied together by using convolution operation and the result of this multiplication is another array of numbers which have the same dimensionality these two matrices. This can be used to obtain a simple linear combination of certain input pixel values in image processing.

In an image processing context, the input arrays of convolution operation are a gray level image and a much smaller matrix of numbers which is known as kernel[2] . Figure 3.1 shows an example image and kernel.

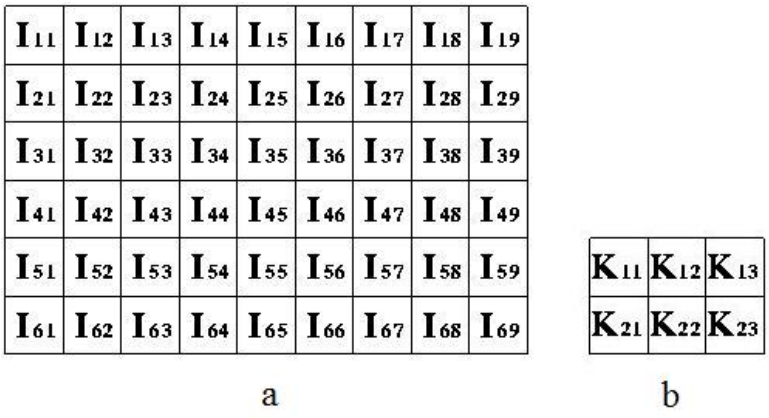


Figure 3.1 A small image (a) and an kernel (b) to illustrate convolution

The convolution is performed by moving the kernel from top left corner of the image through all the positions where the kernel fits entirely within the boundaries of the image. Each position of the kernel corresponds to a single output pixel and value of this pixel is calculated by multiplying together the kernel value and the underlying image pixel value for each of the cells in the kernel, and adding all these numbers together.

By using the sample image and kernel in Figure 3.1 the value of the top right pixel of

[2] A kernel is a smallish matrix of numbers that is used in image convolutions.

the output image is found as follows:

$$O_{17} = I_{17}K_{11} + I_{18}K_{12} + I_{19}K_{13} + I_{27}K_{21} + I_{28}K_{22} + I_{29}K_{23} \tag{3.1}$$

If the image has M rows and N columns, and the kernel has m rows and n columns, then the size of the output image will have $M - m + 1$ rows, and $N - n + 1$ columns.

Mathematically the convolution can be written as:

$$O_{(i,j)} = \sum_{k=1}^{m} \sum_{l=1}^{n} I(i+k-1, j+l-1)K(k,l) \tag{3.2}$$

where i=1 - (M - m + 1) and j = 1 - (N - n + 1).

3.1.2 Sobel Edge Detector

The Sobel operator (SOBEL and FELDMAN, 1973) performs a 2-D spatial gradient measurement on an image. This operation emphasizes regions of high spatial frequency that correspond to edges. Generally it is used to find the approximate absolute gradient magnitude at each point in an input gray scale image.

The operator is a pair of 3x3 convolution kernels as shown in Figure 3.2. One kernel is obtained by rotating the other by 90°.

-1	0	+1
-2	0	+2
-1	0	+1

Gx

+1	+2	+1
0	0	0
-1	-2	-1

Gy

Figure 3.2 Sobel operator

These kernels are designed to respond maximally to edges running vertically and horizontally relative to the pixel grid, one kernel for each of the two perpendicular orientations. The kernels can be applied separately to the input image, to produce separate measurements of the gradient component in each orientation (says Gx and Gy). These can then be combined together to find the absolute magnitude of the gradient at each

point and the orientation of that gradient. The gradient magnitude is given by:

$$|G| = \sqrt{{G_x}^2 + {G_y}^2} \tag{3.3}$$

Typically, an approximate magnitude is computed using:

$$|G| = |G_x| + \left|G_y\right| \tag{3.4}$$

The angle of orientation of the edge (relative to the pixel grid) giving rise to the spatial gradient is given by:

$$\theta = \arctan\left(G_y / G_x\right) \tag{3.5}$$

In this case, orientation 0 is taken to mean that the direction of maximum contrast from black to white runs from left to right on the image, and other angles are measured anti-clockwise from this.

The Figure 3.3 can be given as an example to show the result of the sobel operator.

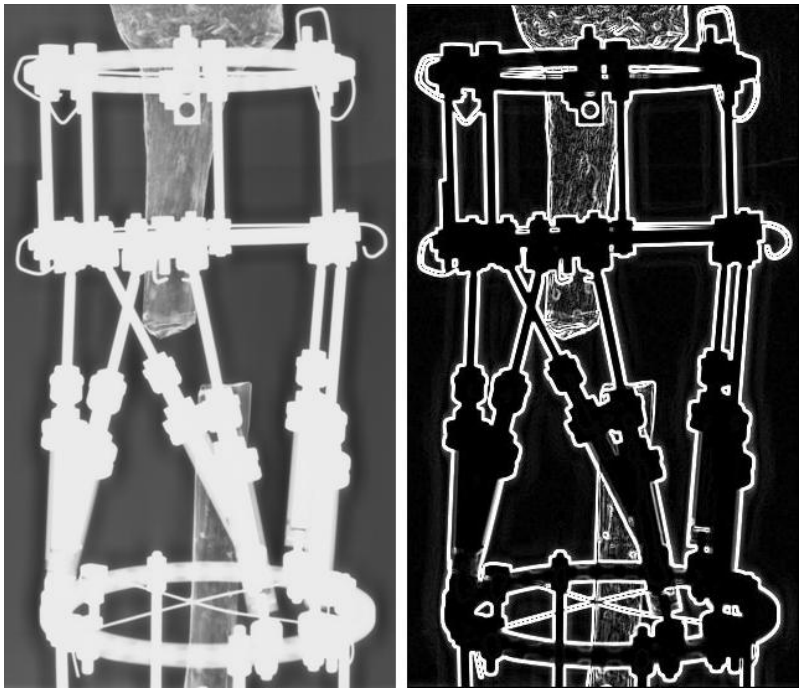


Figure 3.3 A gray scale image and after it is filtered with Sobel operator

3.1.3 Binary Large Object Analysis

A binary large object (blob) (Paul and Horn, 1986) is a group of touching pixels in the same logical state (zero or non-zero). All pixels of the blob are in foreground state

and have non-zero values in a binary image and the others are in a background state and have values equal to zero.

Blob analysis can be used to discover blobs in an image and make measurements of those. This analysis consists of a group of operations that produce information, such as its height or width, number of touching pixels or size, about any 2-D shape in an image.

Blob analysis can be used to find blobs whose spatial characteristics satisfy certain criteria. To keep computation a minimum, blob analysis is a good way to eliminate blobs that are of no interest based on their spatial characteristics, and to keep only the relevant blobs for further analysis.

Another area in which blob analysis is used to find statical information, such as size and number of the blobs, presence, and location of blob regions. These obtained information allows to perform of many machine vision inspection tasks such as detecting flaws on silicon wafers, detecting soldering defects on electronic boards, or web inspection applications such as finding structural defects on wood planks or detecting cracks on plastics sheets (Samad et al., 2005).

If there is a significant variance in the shape or orientation of an object in an application, blob analysis is an effective and plausible way to search for the object. A combination of the measurements obtained through blob analysis can be used to define a feature set that uniquely defines the shape of the object.

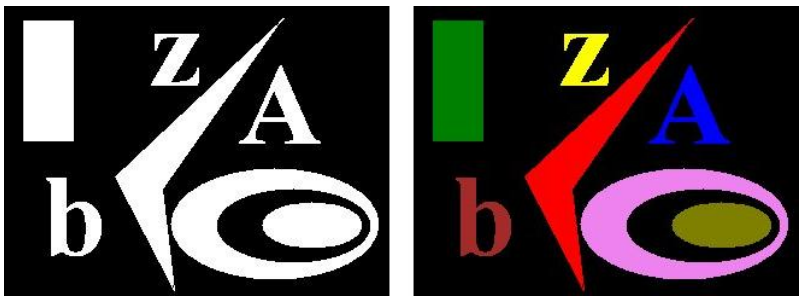


Figure 3.4 A binary image and the result of blob analysis on detecting different objects

Blob analysis is used to eliminate small pixel groups which of no significance to clarify the edges of the bone and external fixator.

3.1.4 Thresholding and Inverting

Thresholding (Gonzalez and Woods, 2002) enables you to select ranges of pixel values in gray scale and color images that separate the objects under consideration from the background. Thresholding converts an image into a binary image, with pixel values of either 0 or 1. This is achieved by assigning 1 to all pixels whose value falls within a certain range, called the threshold interval, and assigning the remaining pixel values in the image to 0.

Inverting (Gonzalez and Woods, 2002) is a pixel based algorithm to obtain negative of an image. For each pixel value extracted from 255 and the new calculated value is negative (inverted value) of a pixel. Inverting algorithm used to invert the colors of the image for obtaining black edges and white background

3.2 Inverse Kinematic Studies

Inverse kinematic analysis consists of these main steps; preparing medical(X-Ray) images, measuring theorical inputs from medical image, obtaining clinical data, using all these inputs in the prepared software, evaluating the results.

3.2.1 Preparing X-Ray Images

It is very important to obtain the medical images as defined in the theory. To do that it is imperative to place the biomechanical system in the right position according to the X-Ray source. Two medical images should be prepared; first one is taken in Antero-Posterior (AP) direction and the second one is taken in the Lateral (L) direction. And the proximal ring for both of the images should be located on the same axis with the x-ray to obtain a suitable reference as defined in the theory; the proximal ring seen as a straight line in the image. And then this analog medical image is digitized by using Vidar Medical Image Digitizer, Figure 3.5. After this preparation step, digitized AP and L images are ready to be measured for obtaining theoretical inputs which are defined in the previous chapter.



Figure 3.5 Vidar medical image digitizer

3.2.2 Measuring Theorical Inputs From Medical Image

The measurement of the theorical inputs which are defined in the previous chapter consists of the following steps:

1. The length of the reference ring (proximal ring) is measured in pixels and divided to its real value in mm to obtain a pixels-length conversion scale. Then this conversion value is tested on a different value which is measured from an object, such as a screw, in the same plane with the reference ring.

2. On the clearest part of the distal ring, a temporary reference line is drawn parallel to the ring. The real reference line is parallel to temporary line and passes through the centers of the spherical joints. The real interval between temporary reference and the real reference is measured and then the corresponding length in pixels is found by multiplying this value with pixel-length conversion scale. Then the real reference is drawn in the right location.

3. The center of the proximal ring is moved to reference axis to find visual center of the ring, G.

4. To obtain the vertical reference line (z- axis), a vertical line to the reference axis is drawn from visual center of the proximal ring.

5. The center line of the proximal fragment of the bone is found by drawing a line from center of the chosen point pairs.

6. The intersection of the proximal bone axis and reference line, G', is found.

7. The length between G and G' is measured.

8. The end point of the proximal bone axis is marked as K.

9. The length between K and G' is measured and denoted as KG'.

10. The angle between z-axis and proximal bone axis, β', is measured.

11. The center line of the distal bone fragment is found by applying the same process which is used for proximal fragment.

12. The end point of the distal bone axis is marked as ${G_1}'$.

13. The angle between distal bone axis and z-axis, β is measured.

14. The appearance of the distal ring is elliptical. A line is drawn on the long axis of this ellipse to find temporary reference axis of the distal ring. Distal reference axis and its center (G_1) is found by shifting the temporary axis.

15. The intersection of distal reference axis and distal bone axis, ${G_1}''$, is found.

16. The length between ${G_1}'$ and ${G_1}''$ is measured.

17. The parallel and vertical distances between G_1 and ${G_1}''$, according to z-axis is measured.

18. A vertical line to the reference axis of the distal ring is drawn from G_1 and the angle between z-axis and this line, Ψ, is measured.

19. The distance between K and ${G_1}'$ is measured according to the z-axis and proximal ring reference axis.

20. All these parameters are converted to the length dimension by using pixel-length conversion scale.

When this algorithm is applied to the L image these theorical inputs are found in the given order: q_y, b_L, β'_L, β_L, c_L, r_y, r_z, Ψ_L, e_y, e_z and if this algorithm applied to the AP image these theorical inputs have been found in the same sequence: q_x, b_{AP}, β'_{AP}, β_{AP}, c_{AP}, r_x, r_z, Ψ_{AP}, e_x, e_z.

Some of the parameters are common to both of the images. These common parameters can be used as control parameters between AP and L images.

3.2.3 Obtaining Clinical Data

Most of the parameters are measured from medical images, but some of them should be obtained by clinical observation. These are the radii of proximal and distal rings, R and R_1, the angular positions of the proximal and distal joints, $\alpha_1 - \alpha_6$ and $\varepsilon_1 - \varepsilon_6$, the angular rotation of proximal ring according distal ring around z-axis, δ_0, and the angular rotation of proximal fragment according distal fragment around z-axis, δ_{Ax}. The measurement of angular positions of the joints and length of the rings is easy but another algorithm is needed to measure δ_0 and δ_{Ax}:

1. The proximal and distal reference axes (x and u) are marked on the ring.
2. Two different wires are mounted on the bone fragments to show anatomic directions of the fragments.
3. An axial photo of the proximal ring of the stabilized biomechanical system is taken.
4. δ_0 is measured from the marks on the rings.
5. δ_{Ax} is measured from the wires.

3.2.4 Evaluating The Results

The link lengths for initial and aligned positions have been obtained by using theorical inputs of medical images and clinical inputs. These theorical outputs are $L_1 - L_6$ for initial position, $L_{1n} - L_{6n}$ for aligned position and b, c for bone fragments.

There are two main sources which effect theorical results; preparing medical images and image processing steps. The medical image should be prepared as defined in the

section “Preparing X-Ray Images” of this chapter. Some parts of the bone fragments which are used in measuring step can't be seen because of the biomechanical system. To overcome this problem some of these parts are chosen approximately. The errors which occur in these steps will cause to unexpected results. Hypotethic examples show that if the theorical inputs are measured exactly the results will be as expected.

Root Mean Square Error (RMSE) is used to calculate over all error of the biomechanical system. The definition of RMSE is

$$RMSE = \frac{1}{6}\sqrt{\sum_{i=1}^{6}(P_i - T_i)^2} \tag{3.6}$$

P_i is used for calculated and T_i is used for expected vaules of the link lengths.

The calculated error shows the overall error of the biomechanical system which is caused from preparing X-Ray image and from image processing steps.

3.3 Fixator Automation Software

Fixator Automation Software is prepared as a part of this thesis. Main purpose of the software is data acquisition and mathematical calculations of the theory. The steps for obtaining the link lengths of initial and aligned states can be defined as follows:

1. Opening the *AP* and *L* medical images from file menu, Figure 3.6
2. Preparing the image for measurement, Figure 3.7
    - Sobel Edge Detector; it is used to find the edges of the biomechanical system.
    - Blob Analysis; it is used to remove small parts of the image to clarify the edges.
    - Thresholding and Inverting; these two filters are used to binarize the image and inverting the colors.
3. Automatic measurement of the parameters, Figure 3.8 and Figure 3.9:

    After image processing steps, the edges of the biomechanical system and bone fragments are obtained. The measurement should be done from these edges, because of

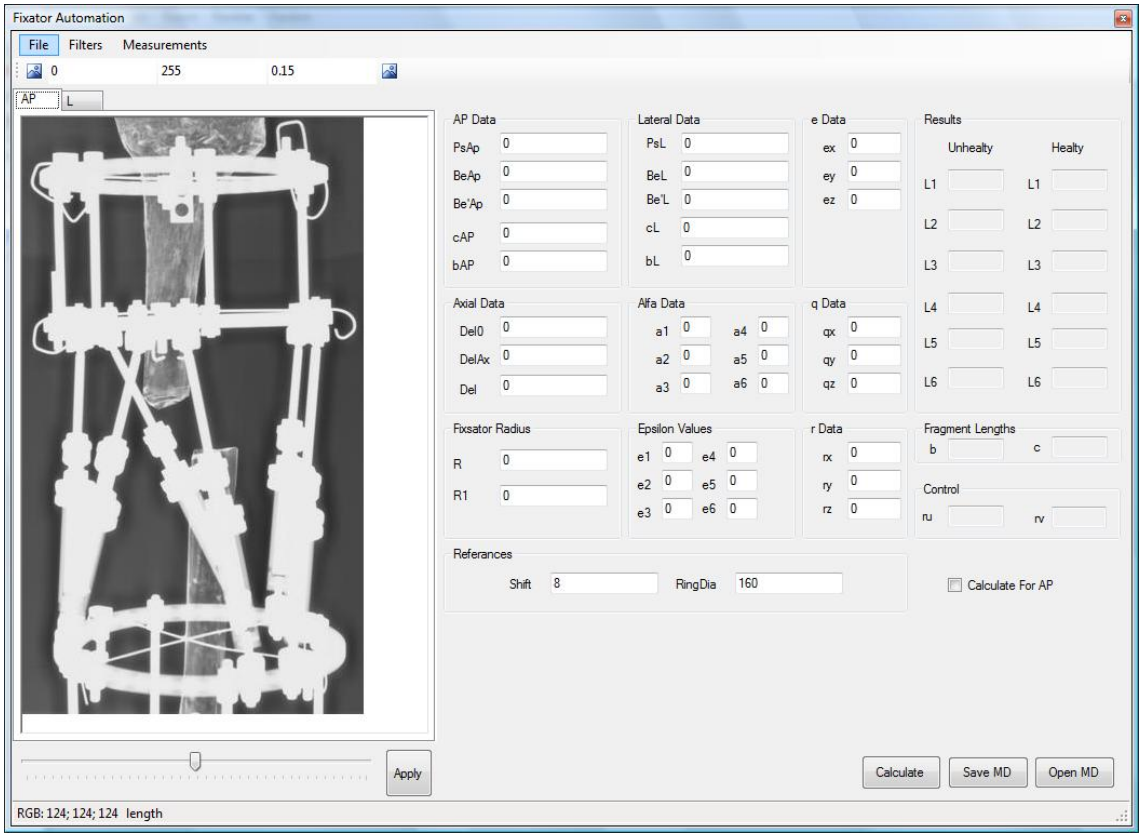


Figure 3.6 The *AP* image and software interface

this reason the software is designed to force the user to choose reference points on these edges so the input parameters can be measured more accurately.

- There are two input boxes; one to enter the diameter of the proximal ring which will be used to obtain length-pixel conversion scale and the other to enter the distance between proximal ring and spherical joints which will be given the ability of making measurements for different kind of fixator assemblies.
- Two points should be chosen on the proximal ring. The first one is on bottom-left corner and the second one is on bottom-right corner of the proximal ring edge. After these two points have been chosen these operations will be performed automatically; firstly the temporary reference axis is drawn, secondly this temporary axis is shifted to obtain general reference axis, thirdly the center of the general axis is found and the z-axis is drawn from this point as a vertical line and finally the length-pixel conversion scale is found by dividing the distance between these two points to the real diameter of the proximal

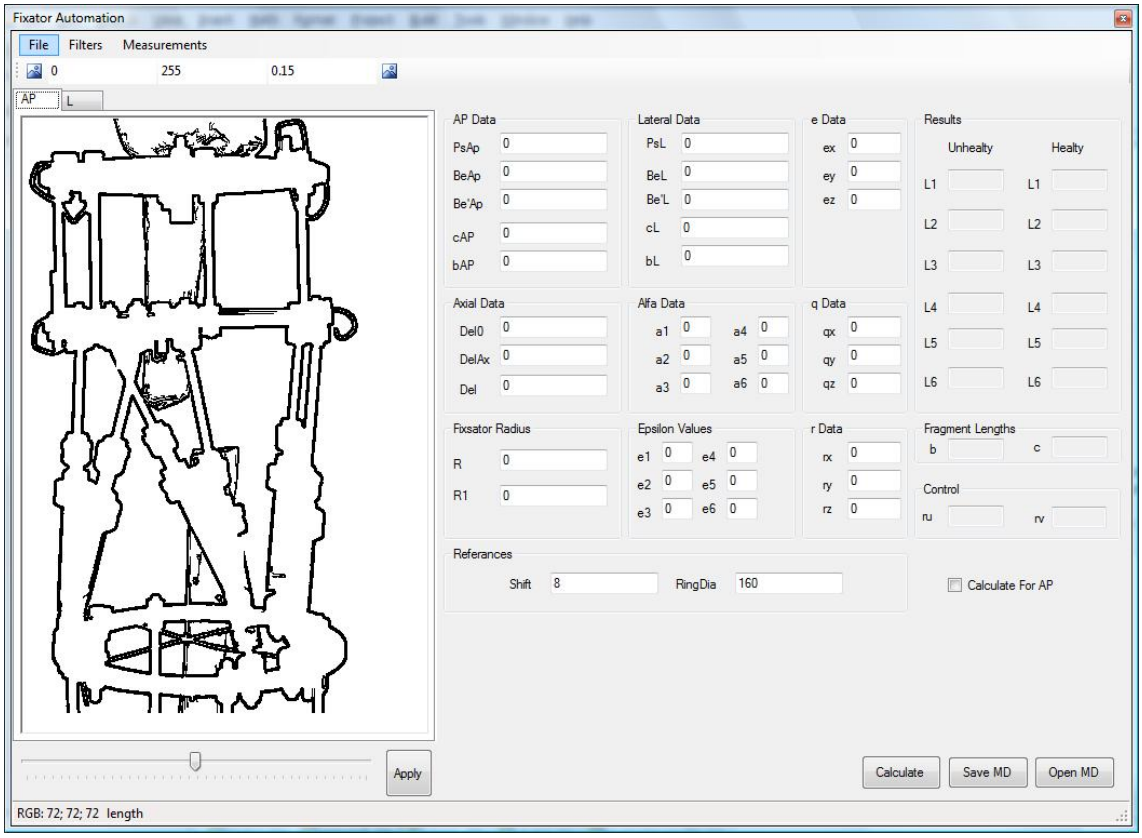


Figure 3.7 The filtered *AP* image

ring.

- At this step totally four point should be chosen; two of them are on the left edge of the proximal bone fragment and the other two pints on the right edge of this bone fragment and on the same level with first two points. By choosing these points the following operations are performed automatically; the bone axis is drawn, the intersection of bone axis and general reference axis is found and the distance between the intersection point and the center point of the general axis is measured and finally the angle between bone axis and z-axis is measured. After this step; q_x, q_z and β'_{AP} values from the *AP* image and q_y, β'_L values from the *L* image are measured automatically and entered in the related input boxes.

- For this step two points should be chosen on distal ring; the first one is on top-left corner and the second one is on top-right corner of the distal ring edge. After these two points have been chosen the following operations are

performed automatically; the temporary distal ring axis is drawn, and this axis is shifted to obtain distal ring axis, the center of the distal ring is found and the w-axis is drawn as a vertical line from this point, the angle between w and z axes is measured. After this step Ψ_{AP} value from AP image and Ψ_L value from L image are measured automatically and entered in the related input boxes.

- At this step totally four point should be chosen on the edges of the distal ring; two of them are on the left edge of the distal bone fragment and the other two pints on the right edge of this bone fragment and on the same level with first two points. By choosing these points the following operations are performed automatically; the bone axis is drawn, the intersection of bone axis and distal ring axis is found and the distance between the intersection point and the center point of the distal ring axis is measured and finally the angle between bone axis and w-axis is measured. After this step, r_x, r_z and β_{AP} values from the AP image and r_y, β_L values from L image are measured automatically and entered in the related input boxes.
- At this step the end points of the both proximal and distal bone fragment axes are chosen; after this step b_{AP}, c_{AP}, e_x, e_z values from AP image and b_L, c_L, e_y values from L image are measured automatically and entered in the related input boxes.
- As final step the clinical data is entered in the related input boxes manually and the calculate button is pressed to obtain final link lengths for initial and aligned states. Some of the parameters are common for both of images and the calculations are normally made for L but if the AP data is more accurate the calculations can be made for AP by checking “Calculate for AP” box.

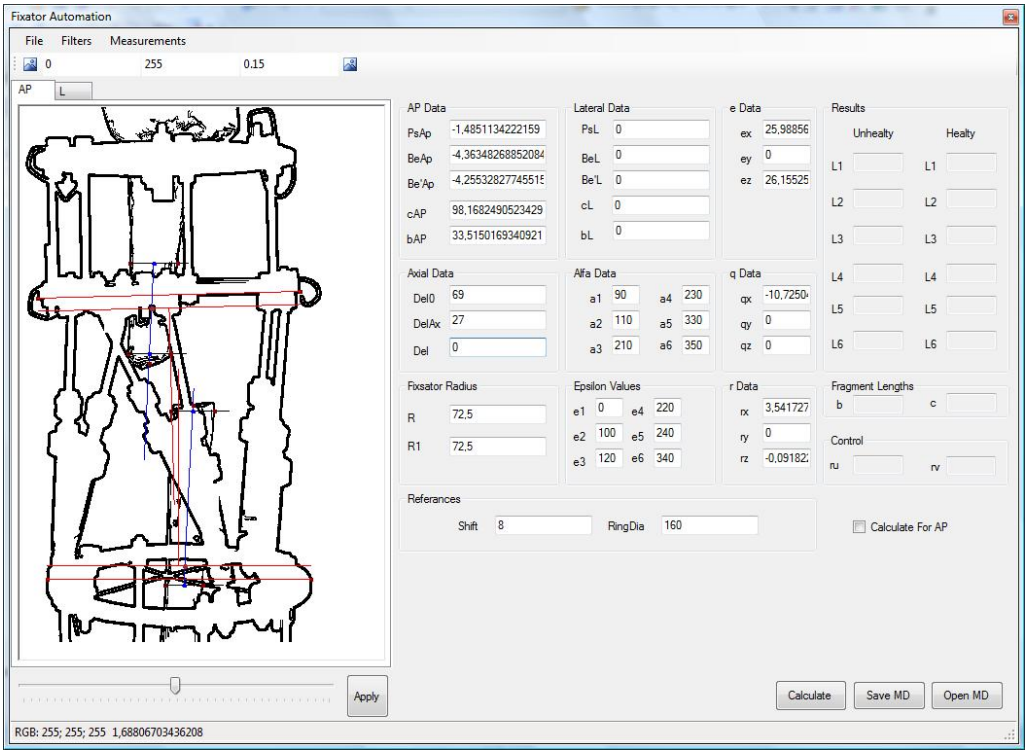


Figure 3.8 The measured *AP* image

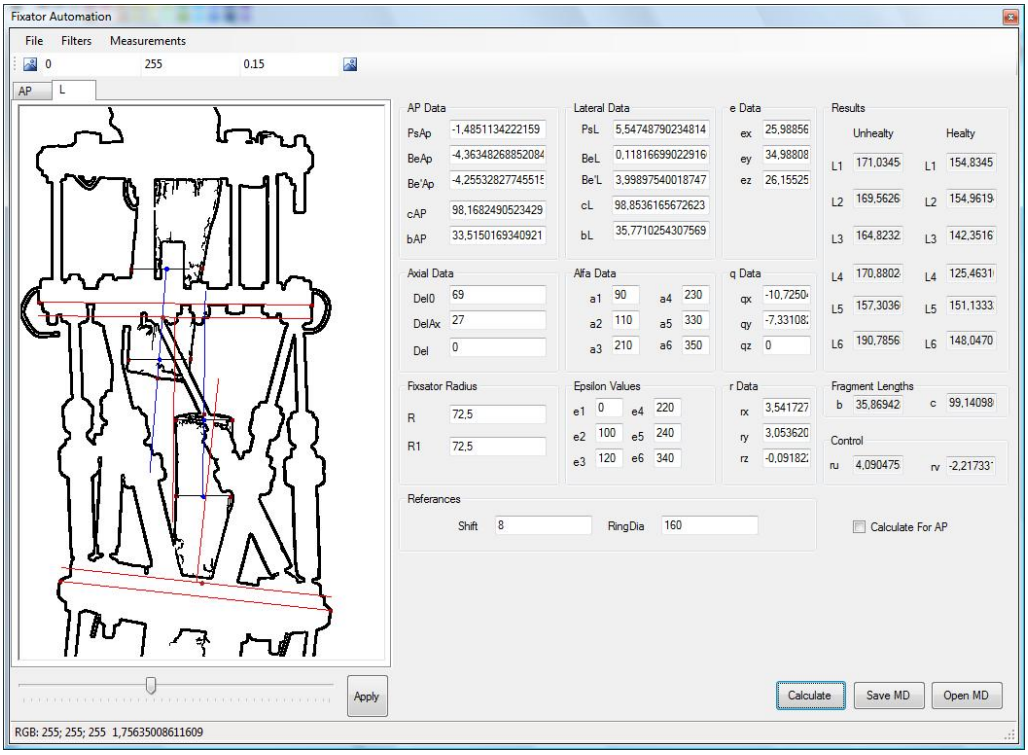


Figure 3.9 The measured *L* image and calculation results

4. RESULTS and DISCUSSIONS

The prepared software at the end of this thesis consists of two main parts. The first part is making the calculations of the theory explained in the previous section and the second one is to make measurements on the medical images to obtain theorical inputs. The experimental work has been done in two steps; first step is verifying the new mathematical theory about inverse kinematics of the biomechanical system based on the old theory (Mutlu et al., 2006) and the second step is comparing the measurements which have been done automatically with the new software and manually with other image processing softwares.

4.1 Verifying the Mathematical Theory

The aim of this numerical experiments is to verify the accuracy of the software for calculating the initial and aligned positions by using the mathematical theory 2. To achieve this purpose the proved numerical examples of the previous theory (Mutlu et al., 2006) have been chosen. The input parameters which are used to test the software are the same with these examples and computed results have been compared with theorical results.

4.1.1 Case 1

This example is about a condition named as case 1. In this case we consider the situation in Figure 4.1. Both bone fragments are perpendicular to the respective circles. The given data for this problem are as following:

The Lateral Data: $e_y = -1.70\,cm$, $e_z = 0.21\,cm$, $c_L = 7.58\,cm$, $b = 12\,cm$, $\beta_L = -12.48^\circ$

The AP Data: $e_x = -2.59\,cm$, $\beta_{AP} = 19.01^\circ$

The Axial Data: $q_x = 0.50\,cm$, $q_y = 0.60\,cm$, $r_x = 0.70\,cm$, $r_y = 0.80\,cm$, $\delta_0 = 60^\circ$, $\delta_{A_x} = -3.87^\circ$

and the expected results are:

$c = 8.00\,cm$, $L_1 = 18.86$, $L_2 = 18.82$, $L_3 = 22.50$, $L_4 = 22.58$, $L_5 = 20.89$, $L_6 = 21.09$

$L_{1n} = 20.80$, $L_{2n} = 20.76$, $L_{3n} = 20.89$, $L_{4n} = 20.80$, $L_{5n} = 20.76$, $L_{6n} = 20.89$

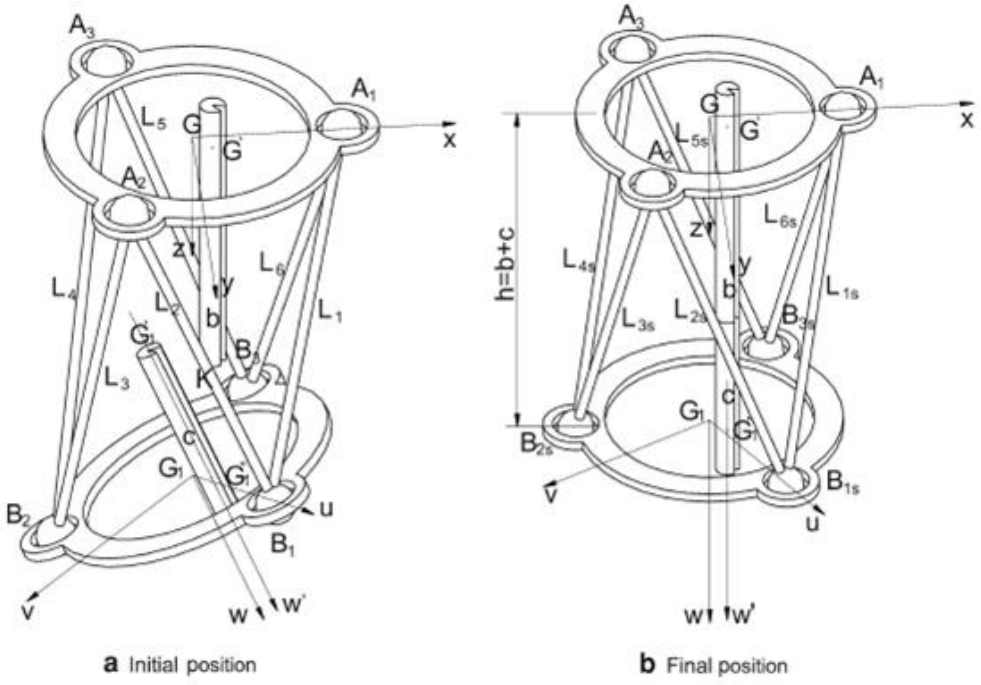


Figure 4.1 Case 1 of fixator assembly

The results of the software for initial and aligned states of Case 1 are:

Initial: $L_1 = 18.88420$, $L_2 = 18.84336$, $L_3 = 22.55330$, $L_4 = 22.60114$, $L_5 = 20.91541$, $L_6 = 21.14532$

Aligned: $L_{1n} = 20.78662$, $L_{2n} = 20.74962$, $L_{3n} = 20.91526$, $L_{4n} = 20.78652$, $L_{5n} = 20.74971$, $L_{6n} = 20.91516$

4.1.2 Case 2

This example is about a condition named as Case 2. The dimensions of the fixator, the *L* and *AP* views, as well as the clinical data, are input to the second case; see Figure 4.2. The given data for this example are as following:

The Lateral Data: $e_y = 1.03\,cm$, $e_z = 1\,cm$, $c_L = 7.05\,cm$, $b = 12\,cm$, $\beta_L = 6.75^\circ$

The *AP* Data: $e_x = -3.58\,cm$, $\beta_{AP} = 28.34^\circ$

The Axial Data: $q_x = 0.50\,cm$, $q_y = 0.60\,cm$, $r_x = 0.70\,cm$, $r_y = 0.80\,cm$, $\delta_0 = 60^\circ$, $\delta_{A_x} = 20^\circ$

and the expected results are:

$c = 8.00\,cm$, $L_1 = 20.82$, $L_2 = 20.82$, $L_3 = 20.82$, $L_4 = 20.82$, $L_5 = 20.82$, $L_6 = 20.82$

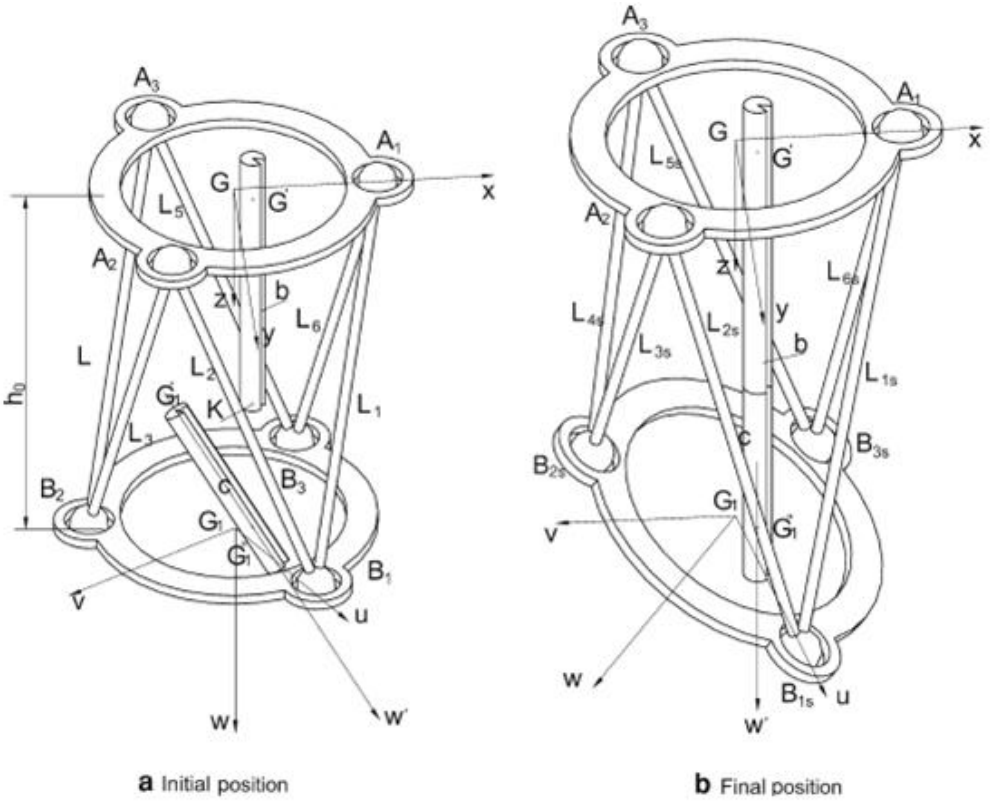


Figure 4.2 Case 2 of fixator assembly

$L_{1n} = 21.10$, $L_{2n} = 21.63$, $L_{3n} = 17.58$, $L_{4n} = 18.32$, $L_{5n} = 21.91$, $L_{6n} = 22.89$

The results of the software for initial and aligned states of Case 2 are:

Initial: $L_1 = 20.81862$, $L_2 = 20.81664$, $L_3 = 20.81797$, $L_4 = 20.81862$, $L_5 = 20.81664$, $L_6 = 20.81797$

Aligned: $L_{1n} = 21.09919$, $L_{2n} = 21.63157$, $L_{3n} = 17.57890$, $L_{4n} = 18.31280$, $L_{5n} = 21.90784$, $L_{6n} = 22.89033$

4.1.3 Case 3

This example is about a condition named as Case 3, Figure 4.3. The physical dimensions, the Lateral, radiographic data and the clinical examination results are the basic input, while the point coordinates, as well as the fracture opening are the required output corresponding to the third case.

The Lateral Data: $e_y = 3.11\,cm$, $e_z = 1.58\,cm$, $c_L = 7.05\,cm$, $b = 11.61\,cm$, $\beta_L = 6.75°$, $\beta'_L = 10.35°$

The AP Data: $e_x = -6.64\,cm$, $\beta_{AP} = 28.34^\circ$, $\beta'_{AP} = 15.00^\circ$

The Axial Data: $q_x = 0.50\,cm$, $q_y = 0.60\,cm$, $r_x = 0.70\,cm$, $r_y = 0.80\,cm$, $\delta_0 = 60^\circ$, $\delta_{A_x} = 20^\circ$

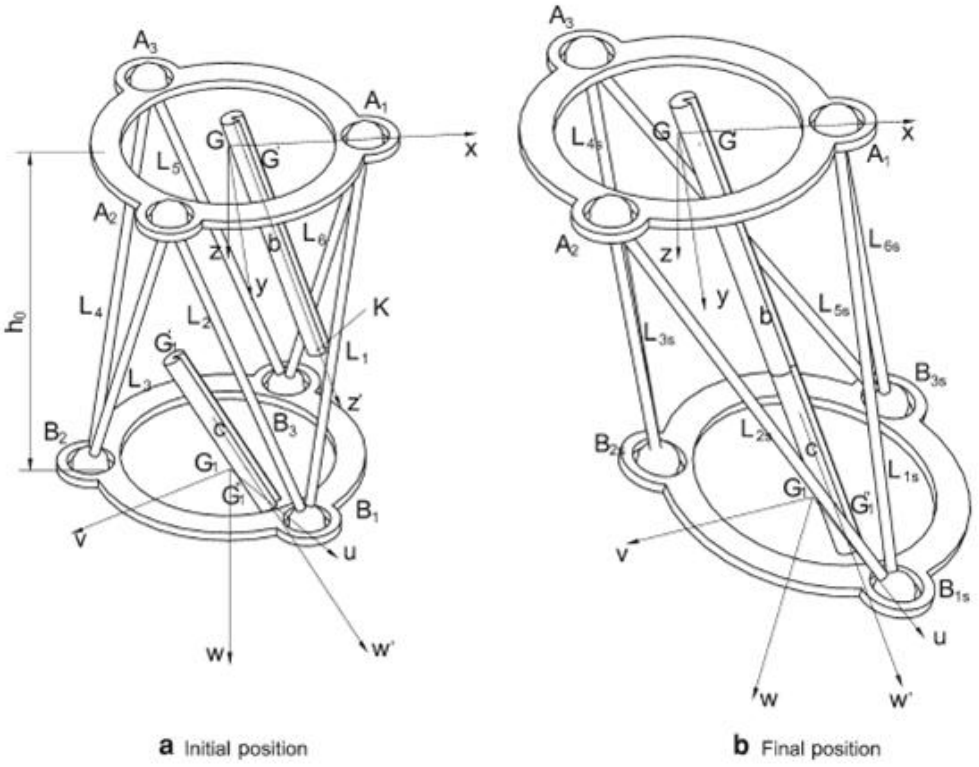


Figure 4.3 Case 3 of fixator assembly

and the expected results are:

$c = 8.00\,cm$, $b = 12.00\,cm$, $L_1 = 20.82$, $L_2 = 20.82$, $L_3 = 20.82$, $L_4 = 20.82$, $L_5 = 20.82$, $L_6 = 20.82$

$L_{1n} = 19.62$, $L_{2n} = 23.15$, $L_{3n} = 19.14$, $L_{4n} = 18.25$, $L_{5n} = 21.78$, $L_{6n} = 21.55$

The results of the software for initial and aligned states of Case 3 are:

Initial: $L_1 = 20.81822$, $L_2 = 20.81776$, $L_3 = 20.82038$, $L_4 = 20.81822$, $L_5 = 20.81776$, $L_6 = 20.82038$

Aligned: $L_{1n} = 19.62643$, $L_{2n} = 23.15273$, $L_{3n} = 19.13958$, $L_{4n} = 18.25578$, $L_{5n} = 21.78703$, $L_{6n} = 21.55320$

When these examples have been examined the results of the general theory and the results of the previous theory (Mutlu et al., 2006) which are used for three different cases,nearly the same. The maximum error of the results is about %0.1 and this error

Table 4.1 Original link lengths for measurement 1

Link	Aligned Link Lengths	Initial Link Lengths
L_1	182.2	169.0
L_2	190.0	210.5
L_3	174.0	145.0
L_4	186.0	190.5
L_5	171.0	167.7
L_6	168.0	172.0

results from rounding the input parameters.

As a result of these examples we can say that the purpose of verifying the generalized theory and the prepared software has been achieved.

4.2 Measurement Experiments With Fixator Automation Software

There are two examples in which measurements are made manually and also by the outlined automatic procedure and their results are compared are given. The bones are flue in both of the examples so the measurements have been made on unfiltered images.

4.2.1 Measurement 1

The Table 4.1 gives original link lengths for aligned and initial positions of the biomechanical system. The results of the example will be compared with these values.

The AP, L and axial data has been measured from Figure 4.4:

The manually measured values are:

The Lateral Data: $e_y = 3.64\,mm$, $c_L = 96.06\,mm$, $b_L = 61.12\,mm$, $\beta_L = -5.22^\circ$, $\beta'_L = 1.85^\circ$, $q_y = 11.67\,mm$, $r_y = 3.42\,mm$, $\psi_L = -2.58^\circ$

The AP Data: $e_x = 35.04\,mm$, $e_z = -10.03\,mm$, $\beta_{AP} = -9.88^\circ$, $\beta'_{AP} = 8.59^\circ$, $c_{AP} = 95.32\,mm$, $b_{AP} = 62.85\,mm$, $r_x = 12.63\,mm$, $r_z = -0.15\,mm$, $q_x = 5.33\,mm$, $\psi_{AP} = -8.59^\circ$

The Axial Data: $\delta_0 = 66^\circ$, $\delta_{A_x} = -28^\circ$

The α and ε values: $\alpha_1 = \alpha_6 = 10$, $\alpha_2 = \alpha_3 = 170$, $\alpha_4 = \alpha_5 = 260$, $\varepsilon_1 = \varepsilon_2 = 0$, $\varepsilon_3 = \varepsilon_4 = 90$, $\varepsilon_5 = \varepsilon_6 = 220$

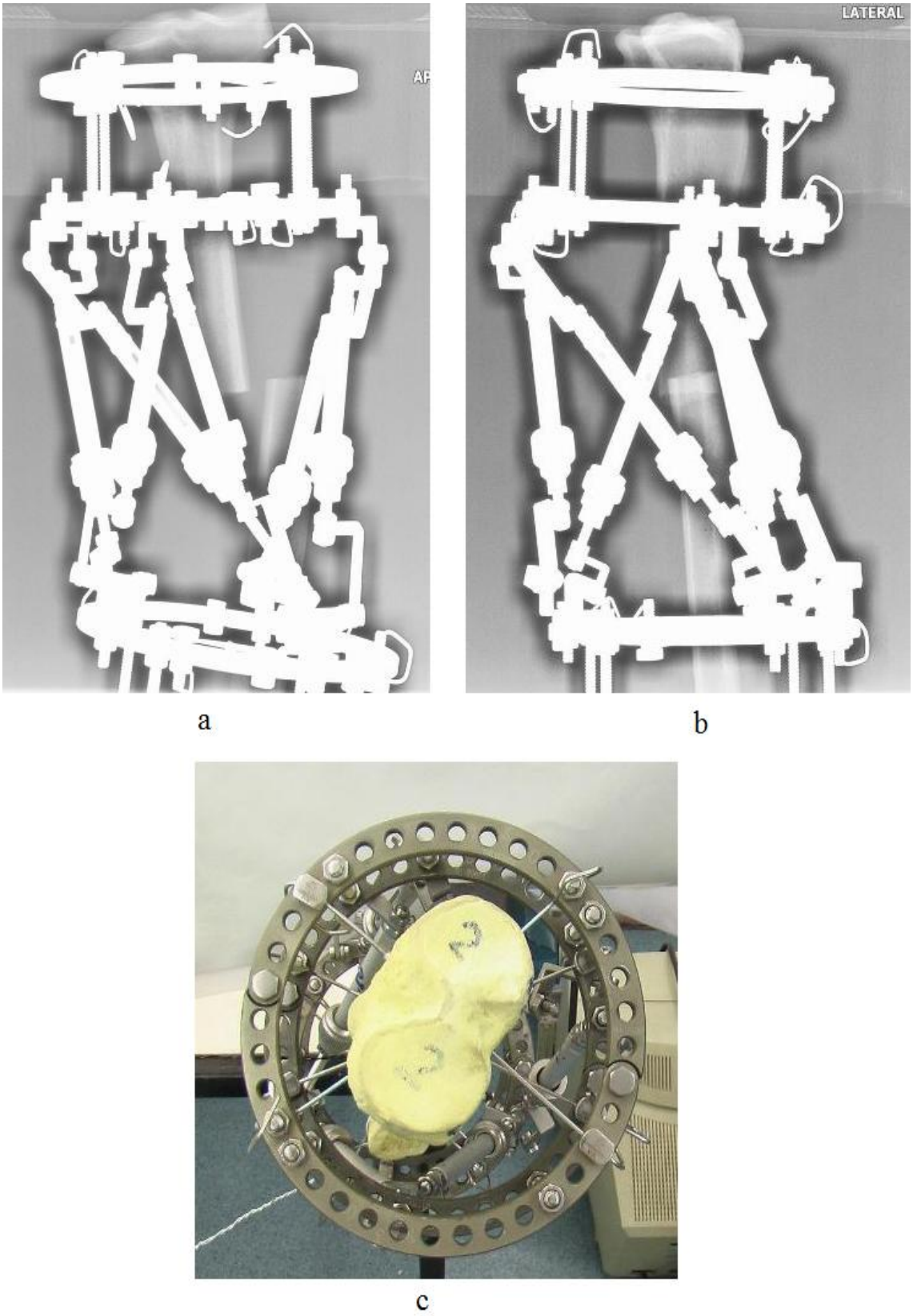


Figure 4.4 The *AP* (a), *L* (b) and Axial (c) images for measurement 1

Table 4.2 Link lengths for initial state of measurement 1

Link	Original Link Length	Manual Calculated	Automatic Calculated
L_1	169.0	166.4553	173.1716
L_2	210.5	204.7324	210.0296
L_3	145.0	142.6984	147.2824
L_4	190.5	183.6505	191.1549
L_5	167.7	162.3616	167.3292
L_6	172.0	168.8496	168.7649

Table 4.3 Link lengths for aligned state of measurement 1

Link	Original Link Length	Manual Calculated	Automatic Calculated
L_1	182.2	182.3687	186.1212
L_2	190.0	194.3823	193.0452
L_3	174.0	174.4043	169.1336
L_4	186.0	187.7445	186.9788
L_5	171.0	167.4313	169.9200
L_6	168.0	161.1922	163.8369

The measurement results of the input parameters with Fixator Automation Software are given in Figure 4.5 and Figure 4.6:

For initial state of the biomechanic system; the original link lengths and calculated link lengths for manual and automatic measurements are given in Table 4.2

The RMSE for initial state of manual measurement is 1.903 and automatic measurement is 0.9699.

For aligned state of the biomechanic system; the original link lengths and calculated link lengths for manual and automatic measurements are given in Table 4.3

The RMSE for aligned state of manual measurement is 1.5048 and automatic measurement is 1.3722.

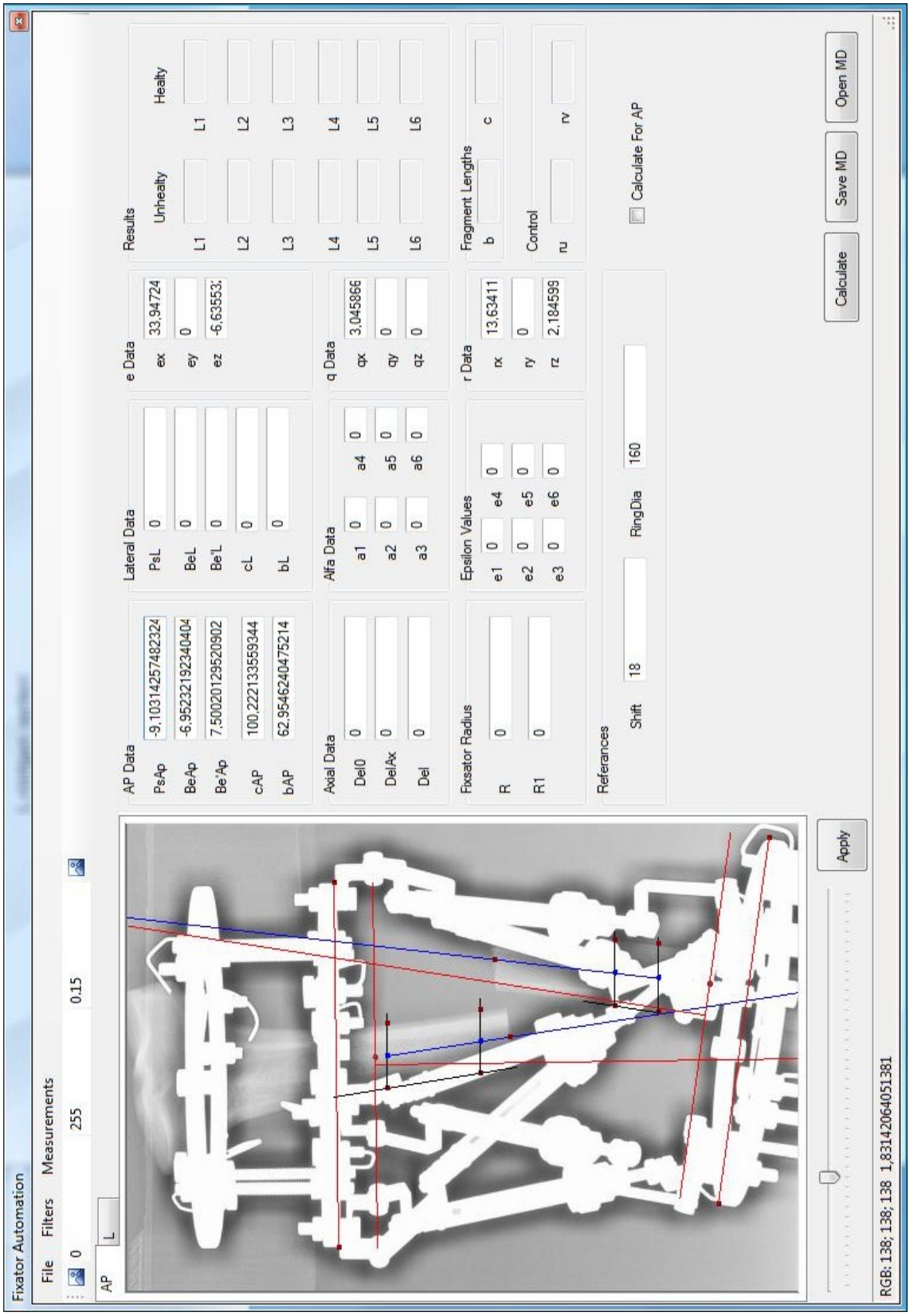


Figure 4.5 The automatic measurement results of *AP* for measurement 1

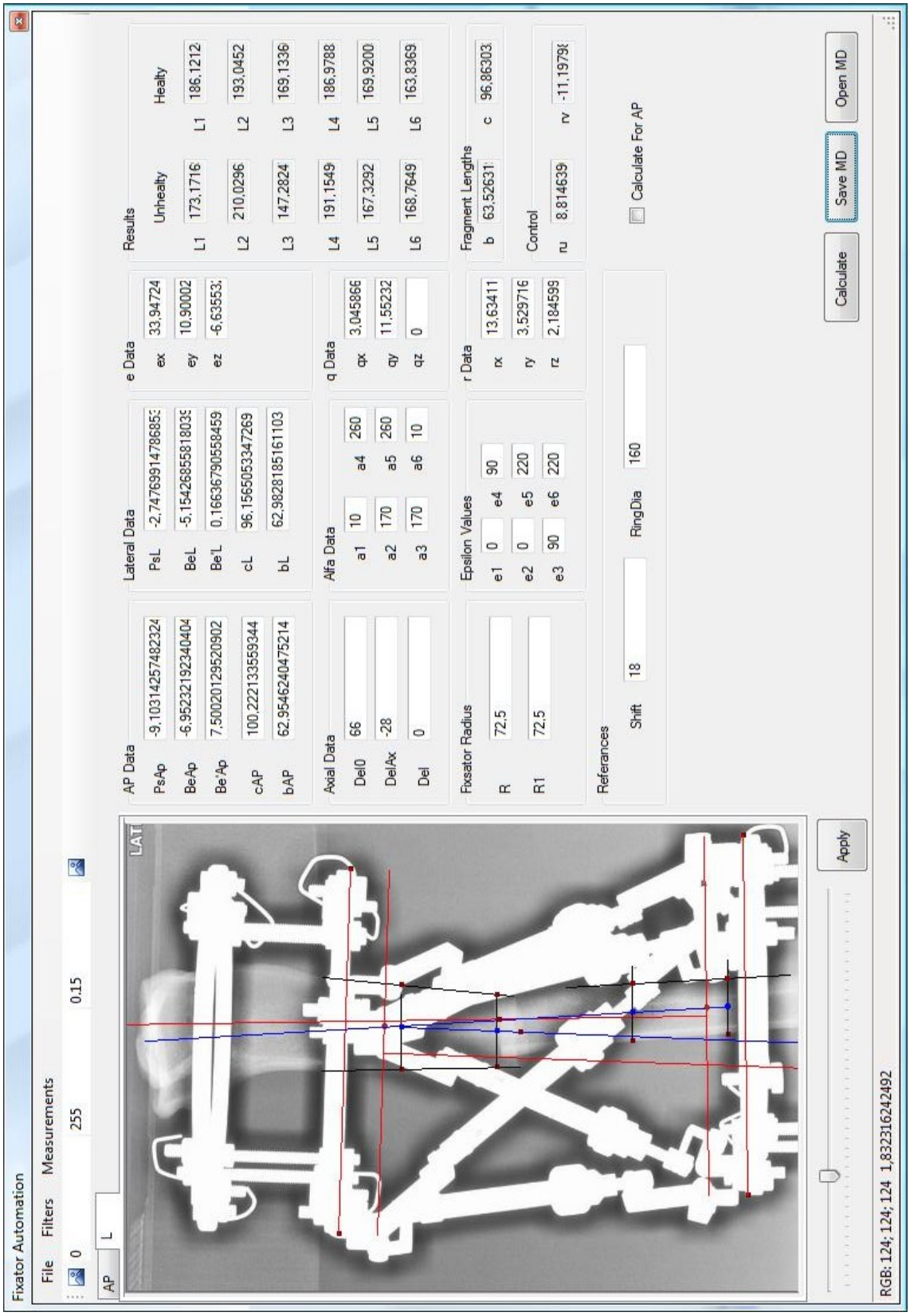


Figure 4.6 The automatic measurement results of *L* for measurement 1

Table 4.4 Original link lengths for measurement 2

Link	Aligned Link Lengths	Initial Link Lengths
L_1	182.2	193.1
L_2	190.0	206.4
L_3	174.0	176.1
L_4	186.0	208.8
L_5	171.0	181.0
L_6	168.0	207.7

4.2.2 Measurement 2

The Table 4.4 gives original link lengths for aligned and initial positions of the biomechanical system. The results of the example will be compared with these values.

The AP, L and axial data has been measured from Figure 4.7:

The manually measured values are:

T The Lateral Data: $e_y = 12.593\,mm$, $c_L = 102.148\,mm$, $b_L = 63.259\,mm$, $\beta_L = -4.13^\circ$, $\beta'_L = -0.5^\circ$, $q_y = 10.593\,mm$, $r_y = 7.333\,mm$, $\psi_L = -1.21^\circ$

The AP Data: $e_x = 5.059\,mm$, $e_z = 15.770\,mm$, $\beta_{AP} = 2.65^\circ$, $\beta'_{AP} = 8.00^\circ$, $c_{AP} = 103.148\,mm$, $b_{AP} = 63.16\,mm$, $r_x = 13.636\,mm$, $r_z = -2.933\,mm$, $q_x = 2.933\,mm$, $\psi_{AP} = -2.57^\circ$

The Axial Data: $\delta_0 = 70^\circ$, $\delta_{A_x} = -17.86^\circ$

The α and ε values: $\alpha_1 = \alpha_6 = 10$, $\alpha_2 = \alpha_3 = 170$, $\alpha_4 = \alpha_5 = 260$, $\varepsilon_1 = \varepsilon_2 = 0$, $\varepsilon_3 = \varepsilon_4 = 90$, $\varepsilon_5 = \varepsilon_6 = 220$

The measurement results of the input parameters with Fixator Automation Software are given in Figure 4.8 and Figure 4.9:

For initial state of the biomechanic system; the original link lengths and calculated link lengths for manual and automatic measurements are given in Table 4.5

The RMSE for initial state of manual measurement is 2.9 and automatic measurement is 2.319.

For aligned state of the biomechanic system; the original link lengths and calculated link lengths for manual and automatic measurements are given in Table 4.6

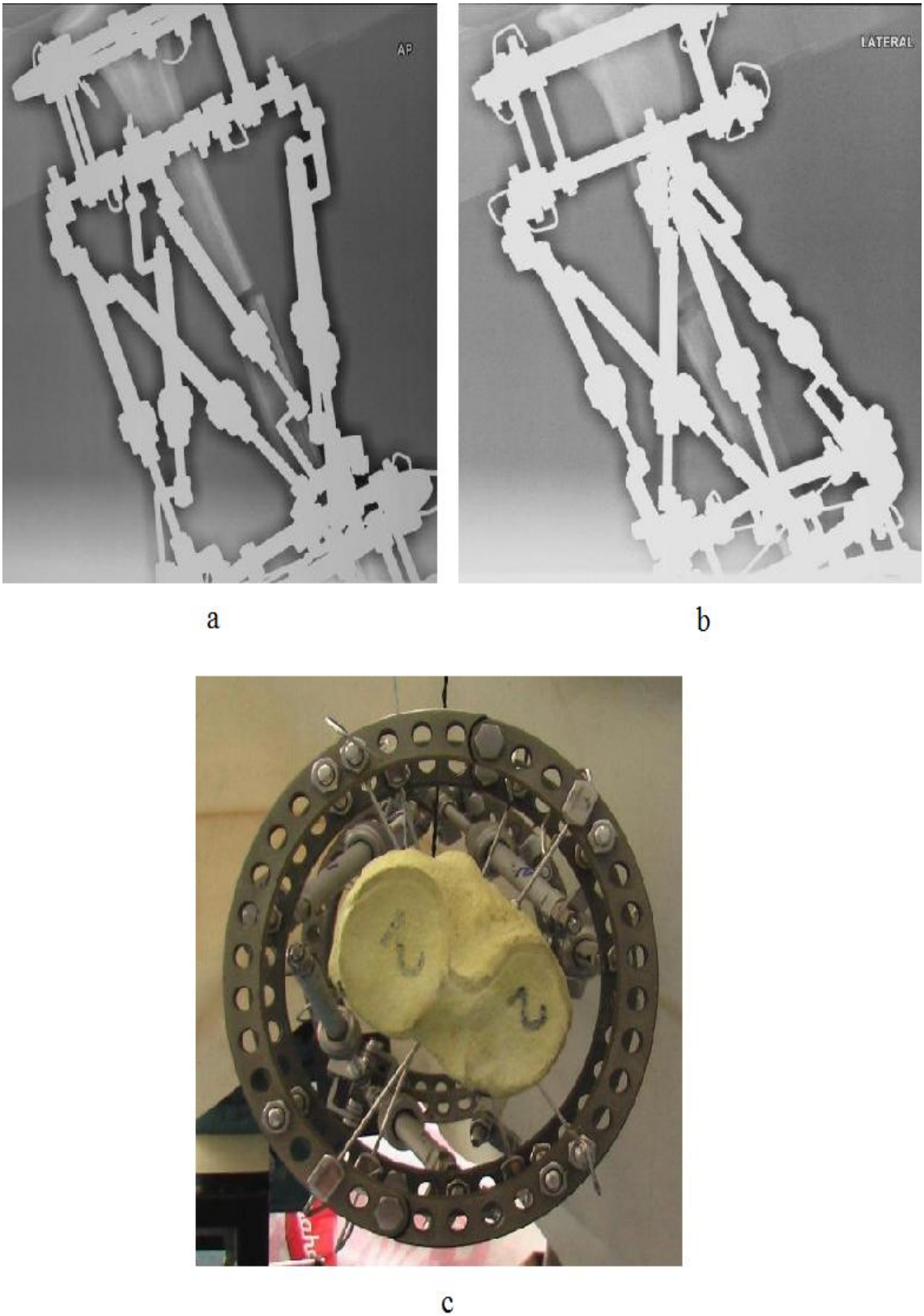


Figure 4.7 The *AP* (a), *L* (b) and Axial (c) images for measurement 2

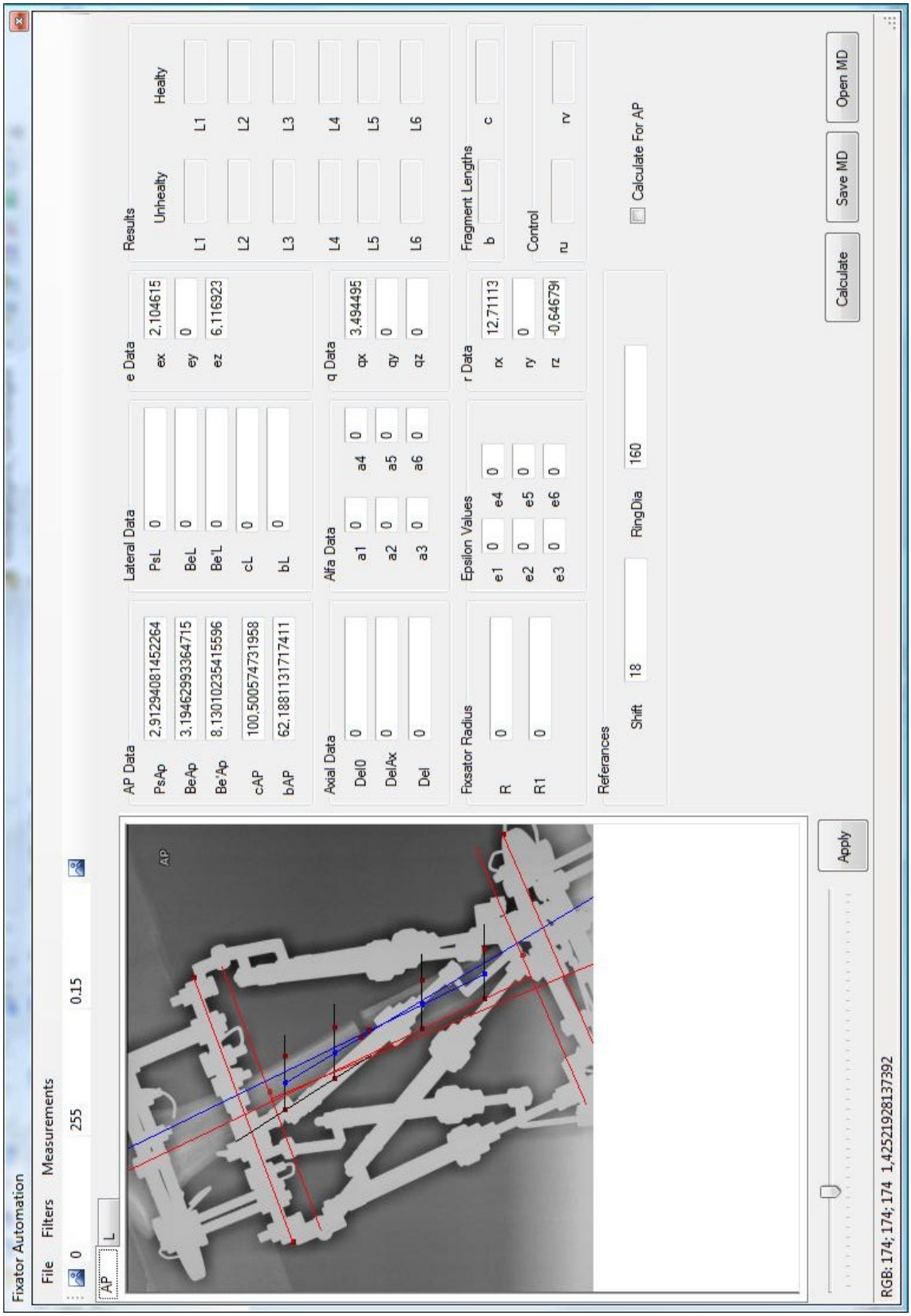


Figure 4.8 The automatic measurement results of *AP* for measurement 2

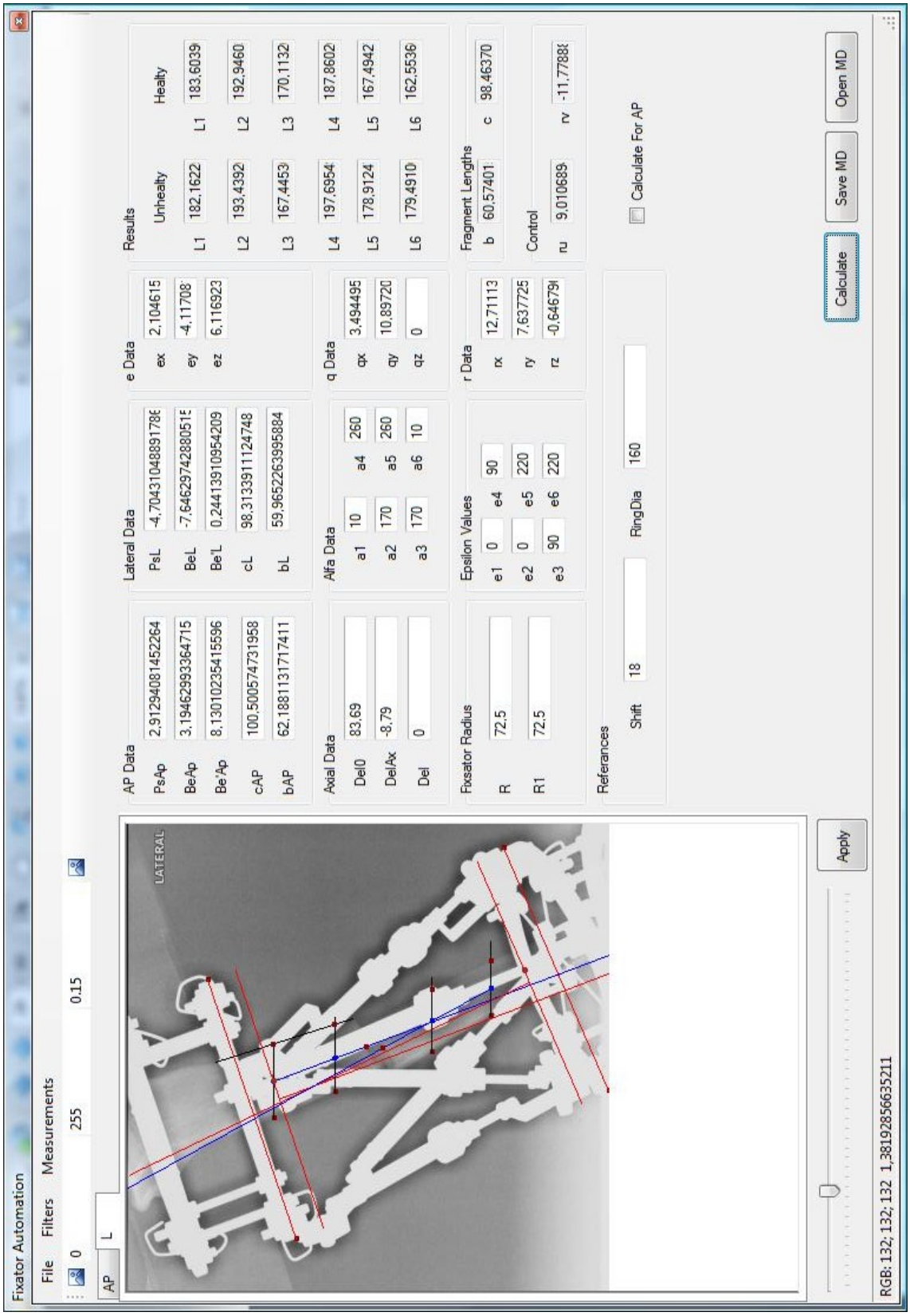


Figure 4.9 The automatic measurement results of *L* for measurement 2

Table 4.5 Link lengths for initial state of measurement 2

Link	Original Link Length	Manual Calculated	Automatic Calculated
L_1	186.6	186.0201	182.1623
L_2	195.3	196.9693	193.4392
L_3	175.3	167.1621	167.4453
L_4	199.0	204.9523	197.6955
L_5	183.0	181.9668	178.9125
L_6	189.0	174.9631	179.4910

Table 4.6 Link lengths for aligned state of measurement 2

Link	Original Link Length	Manual Calculated	Automatic Calculated
L_1	182.2	184.4461	183.6039
L_2	190.0	189.4279	192.9460
L_3	174.0	166.3136	170.1132
L_4	186.0	191.9625	187.8603
L_5	171.0	172.4700	167.4943
L_6	168.0	164.1357	162.5537

The RMSE for aligned state of manual measurement is 1.803 and automatic measurement is 1.406.

These two measurement examples show that the Fixator Automation Software lets us measure the input parameters with higher accuracy and faster. It was taking more than 6 hours to measure these input parameters manually but now it takes just 5-6 minutes to measure them with fixator automation software. When results of these measurements compared with original values, we can say that the error rate of the software is in a acceptable range.

5. CONCLUSION

At the end of this thesis a software has been prepared. This software can be used for medical image processing, data acquisition and mathematical calculations. After image processing steps, the edges of the biomechanical system and bone fragments are obtained. The measurement should be done from these edges, because of this reason the software is designed to direct the user to choose reference points on these edges so the input parameters can be measured more accurately.

The numerical examples of experimental work shows that the new generalized theory covers the old one and the software can be used for calculations of this theory. And the measurement examples show that; the manual measurement of input parameters was taking more than six hours but now it takes just five or six minutes to measure them with the software and the accuracy of the measurements has been improved so the results have been increased gradually in quantity. So finally we can say that the efficiency of the fixator automation has been improved.

REFERENCES

AKÇALI, İ., D., 2007. Tubitak 106m466 project report #1. Technical report, Mactimarum.

BEHRENS, F., 1981. External Skeletal Fixation. *American Academy of Orthopaedic Surgeons Instructional Course Lectures*, 30.

BURNY, F., BOURGOIS, R.,, and DONKERWOLLCKE, M., 1982. Elastic Fixation: A Biomechanical Study of the Half-Frame. *Concepts in External Fixation. New York, Grune and Stratton*, pages 67–68.

ÇAKMAK, M., and KOCAOĞLU, M., 1999. *Ilizarov cerrahisi ve prensipleri*. Doruk Grafik.

CRAIG, J., 1989. Introduction to Robotics Mechanics and Control, Addison-Wesley. *Reading, MA*.

EREN, A., and ERALP, L., 1999. İlizarovsisteminindünyadave Türkiyedeki gelişimi. In ÇAKMAK, M., and KOCAOĞLU, M., editors, *İlizarov cerrahisi ve prensipleri*, pages 1–4, İstanbul. Doruk Grafik.

FERNANDEZ, A., A., 1985. External fixation of the leg using unilateral biplanar frames. *Archives of Orthopaedic and Trauma Surgery*, 104(3):182–186.

FU, K., S., GONZALEZ, R., C.,, and LEE, C., S. G., 1987. *Robotics: control, sensing, vision, and intelligence*. McGraw-Hill, Inc. New York, NY, USA.

GIARRATANO, J., C., and RILEY, G., 1994. *Expert systems: principles and programming*. PWS Publishing Co. Boston, MA, USA.

GONZALEZ, R., C., and WOODS, R., E., 2002. *Digital image processing, 2. Ed.* Prentice-Hall Inc., New Jersey.

ILIZAROV, G., A., and GREEN, S., A., 1992. *Transosseous osteosynthesis: theoretical and clinical aspects of the regeneration and growth of tissue*. Springer Verlag.

MUTLU, H., AKÇALI, İ. D.,, and GÜLŞEN, M., 2006. A mathematical model for the use of a Gough-Stewart platform mechanism as a fixator. *Journal of Engineering Mathematics*, 54(2):119–143.

PARKHILL, C., 1897. A new apparatus for the fixation of bones after resection and in fractures with a tendency to displacement. *Trans. Am. Surg. Assoc.*, 15:251.

PAUL, K., and HORN, B., 1986. *Robot Vision*. The MIT Press, Cambridge, MA, USA.

SAMAD, R., ARSHAD, M. R.,, and SAMAD, Z., 2005. Design of crack detection system software for ic package using blob analysis and neural network. In *ICS'05: Proceedings of the 9th WSEAS International Conference on Systems*, pages 1–6, Stevens Point, Wisconsin, USA. World Scientific and Engineering Academy and Society (WSEAS).

SELIGSON, D., and POPE, M., 1982. *Concepts in external fixation*. Grune & Stratton.

SOBEL, I., and FELDMAN, G., 1973. A 3x3 isotropic gradient operator for image processing. *Pattern Classification and Scene Analysis*, pages 271–272.

CURRICULUM VITAE

I was born in Antakya, Turkey in 1985. I gradueded from Çukurova Universty, Department of Electrical and Electronics Engineering in 2007 and I have been working as a research assistant in the same department since November 2007.